Genome wide sequencing provides evidence of adaptation to heterogeneous environments for the ancient relictual *Circaeaster agrestis* (Circaeasteraceae, Ranunculales)

Running title: Adaptive evolution of *Circaeaster agrestis*

Xu Zhang[1,2,3,#], Yanxia Sun[1,2, #,*], Jacob B. Landis[4,5], Jianwen Zhang[6], Linsen Yang[7], Nan Lin[1,2,3], Huajie Zhang[1,2], Rui Guo[1,2,3], Lijuan Li[1,2,3], Yonghong Zhang[6], Tao Deng[6], Hang Sun[6,*], Hengchang Wang[1,2,*]

[1]CAS Key Laboratory of Plant Germplasm Enhancement and Specialty Agriculture, Wuhan Botanical Garden, Chinese Academy of Sciences, Wuhan 430074, Hubei, China;

[2]Center of Conservation Biology, Core Botanical Gardens, Chinese Academy of Sciences, Wuhan 430074, Hubei, China;

[3]University of Chinese Academy of Sciences, Beijing, 100049 China;

[4]Department of Botany and Plant Sciences, University of California Riverside, Riverside, CA, USA;

[5]School of Integrative Plant Science, Section of Plant Biology and the L.H. Bailey Hortorium, Cornell University, Ithaca, NY USA;

[6]Key Laboratory for Plant Diversity and Biogeography of East Asia, Kunming Institute of Botany, Chinese Academy of Sciences, Kunming, Yunnan, 650201 China;

[7]Hubei Key Laboratory of Shennongjia Golden Monkey Conservation Biology, Administration of Shennongjia National Park, Shennongjia, Hubei, China.

[#]These authors contributed equally to this work.

*****Correspondence: sunyanxia@wbgcas.cn; sunhang@mail.kib.ac.cn; hcwang@wbgcas.cn

Summary

- Investigating the interaction between environmental heterogeneity and local adaptation is critical to understand the evolutionary history of a species, providing the premise for studying the response of organisms to rapid climate change. However, for most species how exactly the spatial heterogeneity promotes population divergence and how genomic variations contribute to adaptive evolution remain poorly understood.
- We examine the contributions of geographical and environmental variables to population divergence of the relictual, alpine herb *Circaeaster agrestis*, as well as genetic basis of local adaptation using RAD-seq and plastome data.
- We detected significant genetic structure with an extraordinary disequilibrium of genetic diversity among regions, and signals of isolation-by-distance along with isolation-by-resistance. The populations were estimated to begin diverging in the late Miocene, along with a possible ancestral distribution of the Hengduan Mountains and adjacent regions. Both environmental gradient and redundancy analyses revealed significant association between genetic variation and temperature variables. Genome-environment association analyses identified 16 putatively adaptive loci related to biotic and abiotic stress resistance.
- Our genome wide data provide new insights into the important role of environmental heterogeneity in shaping genetic structure, and access the footprints of local adaptation in an ancient relictual species, informing conservation efforts.

Keywords: local adaptation, *Circaeaster agrestis*, RAD sequencing, genetic structure, environmental heterogeneity, temperature variables, conservation

Introduction

A primary goal of phylogeography is understanding how geographical and ecological factors shape the genetic structure and evolutionary history of species. Environmental factors can act in concert and vary in space, resulting in divergent natural selection leading to genetic divergence during adaptation to heterogeneous environments (Savolainen *et al.*, 2007). Such genetic divergence along environmental gradients or across varied ecological habitats, can be indicative of local adaptation, a mechanism beneficial to the long-term persistence of populations and intensifying genetic differentiation among populations (Kawecki & Ebert, 2004; Conover *et al.*, 2009; Colautti & Barrett, 2013; Savolainen *et al.*, 2013; Lowry *et al.*, 2019). Understanding the genetic basis of local adaptation will provide insights into the response of organisms to ongoing climate change, aiding in conservation efforts (Aitken *et al.*, 2008; Ahrens *et al.*, 2019).

Divergent natural selection is the driving force of genetic divergence (Darwin, 1859; Coyne & Orr, 2004), while gene flow can buffer genetic differentiation (Spieth, 1974; Goicoechea *et al.*, 2019). Evolution resulting from local adaptation depends on both the strength of local selective pressures and the homogenizing effect of connectivity among different localities. Historically, isolation by distance (IBD) (Wright 1946) have been widely employed in studies of genetic differentiation among populations. Mcrae (2006) proposed the isolation-by-resistance (IBR) model, which predicts genetic connectivity among populations in a complex landscape and provides a flexible and efficient tool to account for spatial heterogeneity, improving the understanding of environmental effect on genetic structuring. Genetic drift may reinforce the establishment and maintenance of genetic differentiation, particularly in populations with small effective size (Wright, 1946; Kimura & Crow, 1964). Quantifying the relative contributions among natural selection, genetic drift and population connectivity to genetic divergence is crucial for understanding the role of local adaptation in adaptive evolution of a species (Savolainen *et al.*, 2007; Friis *et al.*,

2018).

Accessing the molecular basis of local adaptation and identifying selective drivers is still challenging for species with limited genomic resources (Mayol *et al*., 2019). Nonetheless, with advancements in sequencing, it is now possible to study thousands of loci improving our understanding of genome-wide effects of accumulating genetic divergence and genomic properties that influence the process of local adaptation (McCormack *et al.*, 2013; Ellegren, 2014; Seehausen *et al*., 2014; Weigel & Nordborg, 2015). In particular, highly divergent loci identified by Genome-Environment Association (GEA) analyses can be interpreted as potential targets of divergent selection associated with population-specific environmental covariables (Coop *et al.*, 2010; Rellstab *et al.*, 2015; Hoban *et al.*, 2016; Forester *et al.*, 2018). However, for most species, such as relictual alpine herbs, how exactly the spatial heterogeneity promotes population diversification and how genomic variations contribute to adaptive evolution, in particular their interaction, remains poorly understood.

In the present study, we focus on investigating the evolutionary history and local adaptation of *Circaeaster agrestis* Maxim, an annual alpine herb with a relatively narrow habitat (Fu & Bartholomew, 2001; Sun *et al.*, 2017). *Circaeaster* Maxim., with its only alliance *Kingdonia* Balf.f. & W.W. Smith, constitute the early-diverging eudicot family Circaeasteraceae (Ranunculales) (The Angiosperm Phylogeny et al., 2016). Due to special morphological characters such as open dichotomous leaf venation, this genus is of great interest to many botanists (Foster, 1971; Ren *et al.*, 2003). *Circaeaster* exhibits low morphological diversity with only one species, garnering a status of critical endangerment (Wild Plants Under State Protection in China). The distributions of *C. agrestis* is confined to the Qinghai-Tibetan Plateau (QTP) and adjacent areas which exhibit a wide range of elevations from 2,100-5,000 m. The uplift of the QTP has created extraordinarily geomorphological and climatic diversity (Mulch & Chamberlain, 2006). Due to the high mountain barrier formed by the Himalayas in the south, the central and western QTP (i.e. the Himalayas) are

characterized by a cold and dry climate. In contrast, the eastern QTP (i.e. the Hengduan Mountains) and adjacent areas are associated with deep valleys and characterized mainly by a warm and wet climate (Song *et al*., 2010; Tang *et al*., 2013; Lu & Guo, 2014; Favre *et al.*, 2015). Given the high degree of geographical and ecological heterogeneity, the QTP comprises a promising model system for studying genetic signatures of local adaptation.

Mountainous regions like the QTP are often centers of endemism and species diversity hotpots (Myers et al., 2000; Noroozi *et al*., 2018) due to uplift-driven diversification (Hughes & Atchison, 2015; Chen *et al*., 2019). The uplift of the QTP produced diverse habitats facilitating rapid population divergence, but also created geographical barriers leading to isolation and fragmentation of populations (He & Jiang, 2014; Deng *et al*., 2020), the main drivers of species extinction (Hughes, 2017). Therefore, investigating genetic structure and local adaptation of species with a relatively narrow habitat will act as a proxy to comprehensively understand the role of geographical and environmental heterogeneity, while also serving as a pioneer in addressing the issues of small patchy diversity in biodiversity hotspots, aiding conservation and management efforts for threatened species.

Specifically, we generated and analyzed two types of genomic datasets: single nucleotide polymorphisms (SNPs) derived from the restriction site associated DNA sequencing (RAD-Seq) of 18 *C. agrestis* populations and 20 plastome sequences of *C. agrestis* populations with other Ranunculales representatives. We hypothesized that environmental heterogeneity may exert strong selective pressures on *C. agrestis*, driving population divergence and generating genetic variation. The aim of the present study is to illustrate the evolutionary patterns of population divergence interacting with environmental variables and access the potential genetic basis of local adaptation. Here, we raise the following questions: 1) how alpine environments affect genetic structure within species and drive population divergence, and 2) how genetic variation is associated with local adaptation? Answering these questions will help us understand

species adaptation to rapidly changing climate and help to develop sound conservation programs.

Materials and Methods

Sampling, library preparation and sequencing

A total of 139 individuals of *C. agrestis* from 18 localities were sampled (Table S1). Sampling locations were chosen based on existing occurrence records covering the geographic and climatic distribution of the species (Fig. S1). Our field collection followed the ethics and legality of the local government. All voucher specimens were deposited in the Herbarium of Wuhan Botanical Garden (HIB) (Table S1). Total DNA was extracted from silica gel-dried leaves with a modified CTAB (Cetyl trimethylammonium bromide) method (Yang *et al.*, 2014). For RAD library construction and sequencing, genomic DNA was digested with the restriction enzyme EcoRI in a 30 ul reaction followed by ligation of P1 adapter by T4 ligase. Fragments were pooled, randomly sheared, and size-selected to 350–550 bp. A second adapter (P2) was then ligated. The ligation products were purified and PCR amplified, followed by gel purification, and size selection to 350-550 bp. Agilent 2100 Bioanaylzer and qPCR were used to qualify and quantify the library. Paired-end sequencing was performed on two lanes of Illumina HiSeq 2000 at BGI-Shenzhen (Shenzhen, Guangdong, China).

For plastome sequencing, 20 samples representing all 18 localities were chosen. For each sample, a 500-bp DNA TruSeq Illumina (Illumina Inc., San Diego, CA, USA) sequencing library was constructed using 2.5-5.0 ng sonicated DNA as input. The libraries were quantified using an Agilent 2100 Bioanalyzer (Agilent Technologies, Santa Clara, CA, USA) and real-time quantitative PCR. Libraries were multiplexed and sequenced using a 2×125 bp run on one lane of Illumina HiSeq 2000 at BGI-Shenzhen (Shenzhen, Guangdong, China).

Processing of Illumina data

For RAD-sequencing, Illumina reads were processed into RAD-tags using the STACKS v.2.30 software pipeline (Catchen *et al.*, 2013). Samples were initially demultiplexed and filtered with PROCESS_RADTAGS. Reads with an average Phred score of at least 30, an unambiguous barcode, and restriction cut site were retained. The Perl wrapper DENOVO_MAP.PL was used for executing USTACKS, CSTACKS, and SSTACKS (Catchen *et al.*, 2013). Following the suggested protocol (Rochette & Catchen, 2017), we investigated a range of parameter values with M and n values ranging from 1 to 9 (fixing $M = n$) and $m = 3$. We plotted the number of polymorphic loci shared across samples (the r80 loci) and the distribution of the number of SNPs per locus.

The POPULATIONS module in the STACKS pipeline was used to produce datasets for downstream population genetic analyses. Polymorphic RAD loci that were present in all 139 individuals were retained. To validate the influence of missing data, we also employed a filtering parameter of - $r = 0.8$, in which at least 80% of individuals in a population were required to process a locus. Potential homologs were excluded by removing loci showing heterozygosity > 0.5. We further filtered our dataset with a minor allele frequency (MAF) > 0.01 and kept only biallelic SNPs. Finally, we filtered our dataset by selecting the most informative SNP based on the number of minor alleles.

For genome-skimming sequencing, raw sequence reads were filtered using Trimmomatic v.0.36 (Bolger *et al.*, 2014) by removing duplicate reads and adapter-contaminated reads. Remaining reads were directly mapped to the plastome of *C. agrestis* (NCBI accession number: KY908400; plastome size: 151,033 bp) using Geneious v9.0.2 (Kearse *et al.*, 2012). After mapping, the mean depth of coverage was 325.61x (median: 323.55x), ranging from 91.81x (WLG) to 804.08x (ZF). Initial annotations were implemented in the Plastid Genome Annotator (PGA) (Qu *et al.*, 2019), and then refined by manual correction in Geneious. The annotated plastomes

were deposited in GenBank (accession numbers MT228704-MT228722).

Population structure and genetic diversity

Population genetic structure was estimated using Bayesian clustering and principal coordinate analysis (PCoA). Bayesian clustering was performed in STRUCTURE v2.3.4 (Pritchard *et al.*, 2000) with the admixture model. As STRUCTURE analysis assumes that loci are unlinked, we thus filtered out linked SNPs using the *–write_single_snp* option in POPULATIONS (Catchen *et al.*, 2013), which exports only the first SNP per locus for analysis. To determine the optimal number of groups (*K*), we ran STRUCTURE 10 times for $K = 1$ to K = 10. Each run was performed for 200,000 Markov Chain Monte Carlo (MCMC) generations with a burn-in period of 100,000 generations. The optimal *K* was chosen using both delta-*K* method implemented in STRUCTURE HARVESTER (Earl & vonHoldt, 2012), and cross-entropy criterion implemented in *LEA* v2.8.0 (*snmf* function) (https://bioconductor.org/packages/LEA/) (Frichot. & François, 2015). The *snmf* function estimates an entropy criterion that evaluates the quality of fit of the statistical model to the data using a cross validation technique to choose the number of ancestral populations that best explains the genotypic data (Frichot *et al*., 2014). The coefficient for cluster membership of each individual was averaged across the 10 independent runs using CLUMPP (Jakobsson & Rosenberg, 2007) and plotted using DISTRUCT (Rosenberg, 2004). We performed PCoA analyses using *dartR* v1.1.11 (*gl.pcoa* function). We tested the overall population structure using the G-statistic test (Goudet *et al.*, 1996) by *gstat.randtest* function in *adegenet* v2.1.1 (Jombart, 2008). An analysis of molecular variance (AMOVA) was performed to quantify genetic differentiation among and within populations and genetic groups using Arlequin v3.5 (Excoffier *et al.*, 2007) with significance tests of variance based on 10,000 permutations.

We estimated genetic diversity indices including nucleotide diversity (π), expected heterozygosity (H_e), observed heterozygosity (H_o) and inbreeding coefficients (F_{IS})

using POPULATIONS. The polymorphic sites were exported in *Phylip* format and used for calculating haplotypes in DnaSP v6.12 (Rozas *et al.*, 2017). Population and group level F_{ST} using Weir and Cockerham's method (Weir & Cockerham, 1984) was done using *hierfstat* (Goudet, 2005) in R v3.6.1 (R Team, 2014). The absolute differentiation (D_{XY}) among genetic groups were measured using a Perl script provided by Ru *et al.*, (2018) (Li *et al.*, 2020). Finally, we assessed the contemporary effective population sizes (N_e) for each population and group using NeEstimator v2.1 (Do *et al.*, 2014). Estimates of N_e were calculated from the bias corrected (Waples, 2006) linkage disequilibrium method (Hill, 1981) with a minor allele frequency cutoff of 0.05 and 95% confidence intervals (CI) estimated by jackknifing.

Population divergence

We adopted a two-step strategy for investigating the divergent time of *C. agrestis*. First, we used plastome sequences assembled from Ranunculales and newly sampled *C. agrestis* populations to estimate the diversification of *C. agrestis*. A total of 47 plastomes were included. The 79 protein coding regions (CDS) were extracted and aligned using MAFFT v7.313 (Katoh & Standley, 2013) and then concatenated using PhyloSuite v1.1.15 (Zhang *et al.*, 2019). The program BEAST2 v2.5.2 (Bouckaert *et al.*, 2014) was employed for molecular dating with concatenated matrix using a GTR+G+I substitution model selected by jModelTest v2.0.1 (Darriba *et al.*, 2012) under the Bayesian information criterion (BIC). The uncorrelated relaxed-clock mode and birth-death process were applied. The most recent common ancestors (TMRCA) of Ranunculales was constrained to a minimum age of 112 million years ago (Ma) according to the flower fossil assigned to *Teixeiraea lusitanica* von Balthazar, Pedersen & Friis (von Balthazar *et al.*, 2005; Magallón *et al.*, 2015). We set a minimum of 72 Ma to constrain the diverging between Berberidaceae and Ranunculaceae (Anderson *et al.*, 2005; Sun *et al.*, 2018). Following the study of Bell et al., (2010), we modeled both fossil calibrations as an exponential distribution (Ho & Phillips, 2009) with a mean of 1

and an offset (hard bound constraint) that equaled the minimum age of the calibrations. The MCMC was ran for 100 million generations sampling every 1,000 generations. Tracer v1.7.1 (Rambaut *et al.*, 2018) was used to assess the effective sample size (ESS > 200) of each parameter. A maximum clade credibility tree was built by TreeAnnotator v2.5.2 (Rambaut & Drummond, 2010) using median node heights, with the initial 20% of trees discarded as burn-in.

Second, we estimated divergent time between haplotypes of *C. agrestis* using SNP sequences. All the parameters of BEAST2 were kept the same as above, with the exception of the TMRCA of *C. agrestis* constrained based on the previous results. We inferred ancestral distributions of *C. agrestis* using both statistical dispersal-extinction-cladogenesis (S-DEC) (Ree & Sanmartín, 2009) and statistical dispersal vicariance (S-DIVA) (Yu *et al.*, 2010) analyses. Both analyses were implemented in Reconstruct Ancestral State in Phylogenies (RASP) v4.0 (Yu *et al.*, 2015), using 50,000 pruned trees (only *C. agrestis* included) from posterior distribution generated by BEAST2. For both analyses, the number of maximum areas at each node was set to two, and other parameters were left as default. Five biogeographic regions were defined according to the floristic division of China proposed by Wu & Wu (1998) and the phylogeographic study of Lin *et al.*, (2018): A, Qinling-Daba Mountains; B, North Hengduan Mountains; C, North QTP; D, South Hengduan Mountains; E, East Himalayan. To detect potential demographic expansions, temporal changes in the effective population size (N_e) were inferred with Extended Bayesian skyline plots (EBSP) as implemented in BEAST2 (Heled & Drummond, 2008). We used the SNP sequences of 139 individuals and the default substitution model. The MCMC was set to 50 million generations sampling every 5,000 generations, and the first 20% was discarded as burn-in. Final graphs were produced with the custom R script provided by Heled (2010), with a burn-in cutoff of 20%.

Effects of heterogeneous landscapes on genetic structure

To illustrate the effects of the heterogeneous landscapes on shaping genetic structure, we conducted Mantel tests for the presence of IBD and IBR. To avoid the potential correlation between geographical distance and resistance distance, a partial Mantel test was also conducted to test IBD and IBR by controlling the resistance and geographical distance. GenAlEx v6.5 (Peakall & Smouse, 2012) was employed to compute the pairwise geographic distance among 18 populations. Resistance distance was generated in CIRCUITSCAPE v4.0.5 based on circuit theory (McRae, 2006; McRae *et al*., 2008). Circuit resistance provide models of connectivity or resistance to predict patterns of dispersal among sites in a heterogeneous landscape (McRae, 2006; Dickson *et al.*, 2019). The current ecological niche model (ENM) was calculated in MAXENT (Phillips & Dudik, 2008). We used 19 bioclimatic variables available from WorldClim2 (Fick & Hijmans, 2017) at 30 arc□seconds resolution (Table S1), and actual evapotranspiration (AET; http://www.physicalgeography.net/fundamentals/8j.html). To avoid multicollinearity, we ran a Pearson correlation analysis to eliminate one of the variables in each pair with a correlation value higher than 0.9. A total 12 climatic layers was retained for analyses (Table S1).

We used environmental niches representing connectivity between populations as conductance grids to produce pairwise resistance distance, as high habitat suitability was assumed to have low resistance (Nowakowski *et al.*, 2015). Tests of the significance for the relationship between geographical/resistance distances and genetic distance among populations were implemented in *ade4* v1.7 (https://CRAN.R-project.org/package=ade4) using *mantel.rtest* with 9,999 permutations.

Environmental variables and genetic structure

To estimate the contributions of environmental variables to genetic differentiation and to understand the turnover of allele frequencies along an environmental gradient, a gradient forest (GF) analysis was performed using *gradientForest* v0.1

(http://gradientforest.r-forge.r-project.org/). GF is a nonparametric, machine learning regression tree approach that allows for exploration of nonlinear associations of spatial, environmental, and allelic variables (Gugger *et al.*, 2017; Bay *et al.*, 2018). The analysis partitions the allele frequency data at split values along the environmental gradients and defines the amount of variation explained as 'split importance' values (Jiang *et al.*, 2019). The overall predictor importance plot of GF shows the mean importance weighted by allele R^2, and the cumulative plot for each predictor shows cumulative change along the environmental gradient. The split importance values are added cumulatively to produce a step-like curve, thus, areas with large steps in a row indicate significant influence on allelic change. The 12 climatic layers used in above analysis was employed as environmental variables in the GF analysis.

A redundancy analysis (RDA) was performed to understand the associations between genetic structure and environmental variables. We estimated the proportion of genetic variance in the populations that is explained by environmental variables using six important variables identified by GF (bio03: isothermality; AET: actual evapotranspiration; bio04: temperature seasonality; bio07: temperature annual range; bio12: annual precipitation and bio15: seasonality precipitation, see results). We constrained the dependent variables (individuals) by the explanatory variables (climate). The RDA analysis was performed using the *rda* function in *vegan* v2.5 (Oksanen *et al.*, 2018; http://CRAN.R-project.org/package=vegan). The *anova.cca* function was used to calculate overall significance and significance of each climate variable was calculated using 9,999 permutations.

Genome-Environment Association (GEA)

To access the evidence of divergent selection acting on the genome and the genetic signatures of local adaptation, tests of associated outlier loci with environmental variation were carried out using BAYESCENV v1.1 (de Villemereuil & Gaggiotti, 2015), which extends the capabilities of the BAYESCAN algorithm by including a

model that incorporates environmental data. BAYESCENV has been shown to be fairly robust to isolation by distance and a hierarchically structured scenario (de Villemereuil & Gaggiotti, 2015). For a comprehensive consideration of the environmental effect, the environmental covariable layer was calculated with principal component analysis (PCA) of the six important bioclimatic variables, and the first PC axis (PC1), which explained most of the variability (48.62%), was extracted as the input for BAYESCENV. We ran 20 pilot runs of 5,000 iterations and a burn□in of 50,000 iterations, ultimately obtaining 5,000 MCMC iterations for the analysis. Diagnostics of the log likelihoods and F_{ST} values for the 5,000 sampled iterations were checked using *coda* v0.19 (Plummer *et al.*, 2006) to confirm convergence and sample sizes of at least 2,500.

For functional annotation, the locus consensus sequences of all 6,120 SNPs were exported in *fasta* format. Candidate loci identified in GEA were annotated with Blast2Go v2 (Gotz *et al.*, 2008) by searching the non-redundant *Arabidopsis thaliana* protein database with records from the NCBI ESTs databases (Blastx). All the parameters were set as default with e-value < 1.0E-5.

Results

Sequence data processing

We produced 543 gigabyte (Gb) data containing 845,396,236 raw reads for 139 individuals of *C. agrestis* (Table S2). After filtering, the average number of used reads per sample was 4,542,944 (median: 4,883,567; Table S2). The depths of coverage for processed samples ranged from 5.77x (WLG-2) to 22.44x (HZ2-3), with a mean coverage of 11.99x (Table S2). We optimized the parameters for STACKS analysis and obtained the optimal parameters for our dataset to be $M = n = 3$ (Fig. S2). The genome size of *C. agrestis* was estimated to be 1Gb using flow cytometry. After *de novo* assembling, we obtained 3,640,060 loci with mean genotyped sites per locus -144.49bp (a total of c.a. 0.51Gb), which comprises more than half of the genome. After strict

filtering (- r = 1), we obtained 6,959 RAD loci containing 6,120 variant sites that were used for population genetic analyses. The mean genotyped sites per locus was 146.59bp (stderr: 0.03). After a looser filtering (- r = 0.8), we obtained 24,247 RAD loci containing 22,915 variant sites. The sizes of 20 sequenced plastomes from 18 populations of *C. agrestis* ranged from 150,979 bp (ZF) to 151,056 bp (SNJ) possessing the same 79 protein coding genes arranged in the same order (Table S3).

Genetic diversity and structure

We detected an extraordinary difference of genetic diversity at population level, especially for nucleotide diversity (π), which ranged from 0.0008 (HZ2) to 0.1646 (DDL). The expected heterozygosity (H_e) and observed heterozygosity (H_o) were 0.0007 (HZ2) - 0.1555 (DDL) and 0.0014 (HZ2) - 0.2650 (DDL; Table 1), respectively. When a loose filtering strategy was employed, we obtained a similar genetic diversity pattern (Table S4). In total, 66 haplotypes were detected (Fig. 1; Table S5) and the haplotype diversity (H_d) was 0.9798. Genetic differentiation between YL and HZ3 is the highest (F_{ST}=0.9913), and that between ZG and DDL is the lowest (F_{ST}=0.0640; Table S6; Fig. S3a). Estimates of N_e (Table S7) for each population ranged from 0.2 (SNJ, TSM, XLS, DDL) to 1.2 (ZF). Six sites (HZ2, HZ3, KMG, YL, ZG and GS) had negative estimates and infinite 95% CI, which may result from either a truly large N_e or the consequence of limited sampling (Do *et al*., 2014).

We conducted a Bayesian clustering analysis to explore the genetic structure of *C. agrestis*. The delta-K method identified the best-fit number (highest ΔK value) was two (Fig. S4a), referred to the East and West clades hereafter; the cross-entropy criterion indicated a better number of clusters was six (Fig. S4b). Considering the high F_{ST} among populations and the potential bias of ΔK method (Janes et al., 2017), we further subdivided the two clades into two and four groups (E1, E2, W1, W2, W3 and W4), respectively, which was also supported by the PoCA (Fig. 2; Fig. S5). The AMOVA revealed that 77.59% of the overall variation was distributed among six groups, with

11.27% explained by variation among populations within groups (Table S8). Within genetic groups, W2 exhibited the highest nucleotide diversity (π; 0.1646), while W3 had the lowest (0.0206). All genetic groups had lower observed heterozygosity than expected, with the exception of W2. In general, the East clade had lower levels of observed heterozygosity (H_o, E1=0.0029, E2=0.0034, W1=0.0548, W2=0.2650, W3=0.0134, W4=0.0088) and higher levels of inbreeding coefficient (F_{IS}, E1=0.1952, E2=0.1011, W1=0.0384, W2=-0.1806, W3=0.0227, W4=0.0510) than the West clade (Table 1). Both F_{ST} and D_{XY} showed similar patterns of divergence (Table S9 and S10; Fig. S3b), with genetic differentiation between W3 and W4 the highest (F_{ST} =0.8908; D_{XY} = 0.4307), followed by E2 and W4 (F_{ST}=0.8451; D_{XY} = 0.3670), and that between E1 and E2 the lowest (F_{ST}=0.1284; D_{XY} = 0.0620). Estimates of N_e ranged from 0.2 in W2 to 2.1 in E1 (Table S7). The G-statistic test suggested a significant population structure (p = 0.01**; Fig. S3c).

Population divergence

The 47-taxa 79-CDS matrix of Ranunculales used for estimating the original divergence of *C. agrestis* was 66,117 bp in length containing 12,998 parsimony-informative sites. The divergence of *C. agrestis* from *Kingdonia* was estimated to occur in the early Eocene (stem age, ca. 52.19 Ma; 95% highest posterior density [HPD] intervals, 26.12-83.13 Ma), whereas the divergence within *C. agrestis* started in the late Miocene (ca. 6.33 Ma; 95% HPD, 1.96-23.35 Ma) (Fig. S6). The tree topology inferred by BEAST2 using the SNP sequences identified two main clades (East and West clades) and six sub-groups (E1, E2, W1, W2, W3 and W4 groups), consistent with STRUCTURE and PoCA results. The divergence of the two main clades was estimated at appropriately 6.71 Ma (95% HPD, 5.18-7.89 Ma). The subsequent divergence between the six groups occurred mainly during the Pliocene to late Pleistocene (ca. 5.05Ma-2.90Ma) (Fig. 3a). Biogeographic analyses based on both S-DEC and S- DIVA supported Hengduan Mountains and adjacent regions as the most

likely ancestral region for *C. agrestise* (Fig. 3a, 3b and Fig. S7). For the demographic inference, EBSP analysis showed no sign of population expansion or contraction in demographic history of *C. agrestis* (Fig. 3c).

Effects of topography and ecology

Given that the distribution range of *C. agrestis* is topographically complex, we evaluated the influence of the heterogeneous landscape in shaping genetic structure via Mantel tests. Our analyses suggested both significant patterns of IBD (R^2= 0.443, P = 0.001**) and IBR (R^2= 0.315, P = 0.017*) (Fig. 4a and b), which were also supported by a partial Mantel test (R_1^2= 0.426, P = 0.001**; R_2^2= 0.192, P = 0.011*). Geographical distance explained the genetic structure better than resistance distances based on current distribution of habitats. We further plotted the conductance grid derived from the IBR model to illustrate the connectivity among populations and thus predict the probabilities of successful gene flow through a complex landscape. In general, connectivity gaps among populations were observed in the western clade, reflecting increased habitat isolation in this area resulted from complex topography. In contrast, locations of eastern clade had low resistance to dispersal thus high connectivity among populations (Fig. 4c).

Environmental variables associated with genetic structure

Among the 12 variables used for GF analysis, isothermality (bio03) was indicated as the most important predictor. Actual evapotranspiration (AET), temperature annual range (bio07) and temperature seasonality (bio04) were also of high importance. Seasonality precipitation (bio15), and annual precipitation (bio12) showed moderate importance to allele frequencies. The other six environmental variables had lower contributions (Fig. 5a). Fig. 5b shows the cumulative change in overall allele frequencies, where changes evolved with the environmental gradient.

The RDA analysis revealed a significant amount of genetic variation among

populations associated with the six important environmental variables (46.58%, p = 0.001). Each of the two axes explained a significant amount of variation (Axis 1: 58.55%, P = 0.001**; Axis 2: 27.31%, P = 0.001**; Fig. 6). All six environmental variables were ran separately and found to be significant. The contribution on genetic variation of each variable was generally consistent with the GF analysis. Isothermality (bio03; 18.93%, P = 0.001**) was the most important predictor, whereas the temperature annual range (bio07) was less important in RDA analysis (Table 2).

Genome□Environment Association (GEA)

The BAYESCENV result revealed a total of 61 loci having a significant association with environmental variables. Sixteen of the 61 loci were successfully annotated by Blast2Go with cut-off of e-value <1E-5 and a mean similarity more than 80 (Table 3; Table S11). Among these were genes related to abiotic stress response and stress-induced morphological adaptations, such as *UGT74E2* (Loci ID: 2763; Gene Ontology (GO) term: transferase activity) regulating auxin homeostasis (Tognetti *et al*., 2010), *SRK2E* (Loci ID: 8038; GO: protein kinase activity, ATP binding) involved in drought resistance (Mustilli *et al.*, 2002) and *AHK5* (Loci ID: 203056; GO: phosphorelay sensor kinase activity, phosphorelay signal transduction system) regulating stomatal state and transmitting the stress signal (Pham *et al.*, 2012), as well as genes required for the formation and development of leaves and flowers (*CYP71*, loci ID: 293398; GO: regulation of flower development, meristem structural organization leaf formation; *CSI1*, loci ID: 218068; GO: cellulose biosynthetic, pollen tube development) (Li & Luan, 2011). These loci also include genes related to oxidation-reduction process involved in cellular respiration, for example *NDUFS7* (Loci ID: 83859; GO: oxidoreductase activity, NAD binding) and *NDUFB3* (Loci ID: 219291; GO: electron transport chain).

Discussion

Effects of topography on genetic structure

Our study presents the genetic structure of the palaeoendemic alpine *C. agrestis*. High haplotype diversity, uneven distribution of genetic diversity, as well as significant IBD and IBR patterns suggest restricted gene flow is likely a key factor in the high genetic differentiation among *C. agrestis* populations. The distribution area of *C. agrestis* is remarkable for its extraordinarily topographic diversity with some of the world's most rugged mountain ranges and altitudinal gradients spanning over 5,000 m (Wen *et al.*, 2014; Favre *et al.*, 2015). As a direct consequence of the uplift of the QTP, habitat isolation induced by complex topography and frequented climatic fluctuation was invoked as an important mechanism for the high diversity of alpine plants in this area (Wen *et al.*, 2014; Sun *et al.*, 2017). Hence, dramatic terrain and climate changes probably influenced genetic connectivity and shaped current genetic structure of *C. agrestis*.

We explored the number of genetic clusters of *C. agrestis* using delta-*K*, cross-entropy criterion and PCoA analysis. Despite potential bias of delta-*K* method which exhibits a pathology toward *K*=2 (Janes et al 2017), the two distinct clades identified may reflect the early diversification of *C. agrestis*, and correspond to two unique climatic regions (Chen *et al.*, 2018). Both cross-entropy criterion and PCoA analysis indicated fine-scale structure within *C. agrestis*. For conservation purposes, fine-scale genetic structure can provide essential information for *in situ* conservation (Chung *et al.*, 2005). In particular, common garden experiments were found to be infeasible for *C. agrestis* during our field investigation, suggesting *ex situ* conservation strategies impractical.

Although previous studies suggested that drastically different levels of genetic diversity among populations may produce a bias estimate of F_{ST} (Charlesworth, 1998), both F_{ST} and D_{XY} showed similar pattern of genetic differentiation, revealing high isolation in the western clade. Coupled with the significant IBR pattern, habitat isolation, perhaps caused by complex topography, may be the cause for limited gene

flow as well as observed high differentiation. The QTP orogeny likely triggered the vicariance among different *C. agrestis* groups, consistent with the hypothesis of diverse isolated heterogeneous habitats on sky islands (He & Jiang, 2014), which has been reported in other alpine species (e.g. *Ligularia vellerea*, Asteraceae, Yang et al., 2012; *Salix brachista*, Salicaceae, Chen *et al*., 2019; *Ficus tikoua*, Moraceae, Deng *et al*., 2020). The north-south mountain chains and valleys may provide corridors for flora exchange between the north and south but represent barriers to migration between the east and west (Chen *et al.*, 2018); likely resulting in the observed meridional differentiation of *C. agrestis* in the western clade as seen in previous studies (e.g., Gao *et al.*, 2007; Li *et al.*, 2011). Notably, the populations located in the Hengduan Mountains, exhibit high levels of genetic diversity (Table 1), which has been previously observed in plant species, such as *Parasyncalathium souliei* (Asteraceae) (Lin et al., 2018), *Taxus wallichiana* (Taxaceae) (Liu et al., 2013) and *Quercus aquifolioides* (Fagaceae) (Du et al., 2017). As the QTP blocks the cold and dry air (Liu *et al*., 2013), the Hengduan Mountains are characterized by a much warmer and wetter climate, providing a comparatively stable environment. Although the western populations are likely to possess higher genetic diversity, they are also likely to be more vulnerable to shifting disturbance regimes and environmental changes due to lack of genetic connectivity resulted from habitats isolation. Compared to the western clade, north-south mountain barriers among different latitudes may be driving the divergence among the groups in the eastern clade. A conductance grid derived from the IBR model showed low resistance to dispersal, thus high connectivity, among populations in the eastern clade. In addition, E1 and E2 exhibit a relatively low level of genetic differentiation. This phenomenon is likely due to the similar local environments among different populations resulting from the quite moderate topographical and climatic characteristics in this region (Chen *et al*., 2018).

The concept of effective size is key to conservation genetics, as it summarizes population status regarding inbreeding and genetic drift and provides the prospects for

the sustainability of the population (Wang *et al.*, 2016). Although N_e is frequently less than the census population size, small values of N_e combined with low heterozygosity suggest high levels of inbreeding in populations of *C. agrestis*. The reduction of genetic diversity, as well as the fixation of mildly deleterious alleles that reduce reproductive fitness, influences long-term population persistence and poses a risk of extinction (Kramer & Havens, 2009; Oakley & Winn, 2012; Poudel *et al.*, 2014). In addition, episodes of low population size have a disproportionate effect on the overall value of N_e (Charlesworth, 2009). Thus, low N_e may also be attributed to the disturbance caused by human activities or possible bottleneck events in the evolutionary history of *C. agrestis*.

Impact of environmental heterogeneity in population divergence

Our molecular dating based on plastome sequences suggested an early Eocene origin of *C. agrestis*, which is accordant with previous estimates (Ruiz-Sanchez *et al.*, 2012) and recent results from nuclear data (Sun *et al.*, 2020). The diversification of *C. agrestis* has increased since the Pliocene (Fig. 3), which is likely related to intense uplift of the Hengduan Mountains during the late Miocene to late Pliocene (Mulch & Chamberlain, 2006; Sun *et al.*, 2011; Favre *et al.*, 2015). The environmental and climatic fluctuations triggered by mountain uplifts can always lead to divergent selection and species adaptation associated with dramatic ecological niche changes (Ren *et al.*, 2017). Orogenic activities not only provide numerous new habitats favorable for diversification, but also promote population divergence due to hindered gene flow. Our biogeographic analysis revealed that the demographic evolution of *C. agrestis* has not simply been influenced by the orogeny at a particular time in history, but involves repeated episodes of dispersal and subsequent vicariance events. Coupled with the evidence of significant IBD and IBR patterns, we speculate natural selection driven by extraordinary environmental heterogeneity and geomorphological dynamics may have profound impact in the diversification of *C. agrestis*. In addition, during our field work we found the census population sizes of *C. agrestis* in the Himalaya-Hengduan

Mountains to be much smaller than other sites. Previous studies have indicated a significant negative effect of small population size on adaptive evolution (Nevado *et al.*, 2019). Hence, we speculate that natural selection may play double-edged roles in the evolutionary history of any given species. On one hand, heterogeneous environments could provide more new ecological niches conducive for speciation, on the other hand, it may put the populations with weak adaptive ability to new environment in danger of extinction. Furthermore, significant IBR pattern suggest that genetic structure would be better explained by combining habitat isolation between populations than just geographical distance alone. Thus, habitat changes may have large effect on genetic structure for *C. agrestis*, indicating its sensitivity to environmental niche.

Studying local adaptation contributes to understanding the ability of populations to sustain or adapt to rapid climate change (Jia *et al.*, 2019). We associated environmental variables with genetic structure to demonstrate the impact of environmental heterogeneity on population divergence. Specifically, we found a significant association between genetic variation and temperature variables (Fig. 4; bio03, AET, bio04, bio07), suggesting temperature is an important driver of genetic variation within *C. agrestis*, as detected in previous studies of angiosperm trees (Ahrens *et al.*, 2019; Jia *et al.*, 2019; Jiang *et al.*, 2019). In fact, there is growing evidence that high-mountain environments experience more rapid changes in temperature than environments at lower elevations (Pepin *et al*., 2015; Palazzi *et al.*, 2019). Despite that, little attention has been given to understanding the mechanisms of adaptive response to climate change in high altitude areas. *C. agrestis* is habitually confined to grow under trees, shrubs or rocks, indicating sensitivity to temperature. Moreover, the vertical distribution of *C. agrestis* is extensive, ranging from 2,100 to 5,000 meters above sea level (Fu & Bartholomew, 2001), exhibiting a considerable differentiation in temperature. Therefore, it is reasonable that temperature variables play a vital role in promoting genetic divergence within *C. agrestis* and given the ongoing climate warming, temperature is likely to be a key driver for adaptation of *C.*

agrestis in the future.

Genomic signatures associated with local adaptation

BAYESCENV identified a set of genes that may be involved in a continuously adaptive process. Some genes such as pivotal kinases involved in signaling pathway regulation, may induce abiotic stress responses for defense in harsh climates in the QTP. For example, genes associated with abscisic acid (ABA) signaling pathway (*SRK2EA*) can regulate numerous ABA responses, such as stomata closure, to response to high altitudes with extreme difference in temperature (Sierla *et al.*, 2018). Considering the tiny leaves of *C. agrestis*, we speculate that stomatal regulation would be a vital process for maintaining hydration and regulating temperature. As altitude increases, hypobaric hypoxia becomes the main factor interfering with life activity. Genes related to oxidation-reduction processes involved in cellular respiration, such as *NDUFS7* and *NDUFB3*, are of importance in facilitating adaptation of *C. agrestis* to high altitude areas of hypoxia. In addition, some putatively adaptive genes (*CYP71* and *CSI1*) are associated with physiological trait regulation of vegetative and reproductive organs (Gu *et al.*, 2010). Thus, morphological adaptations may be an essential alternative for *C. agrestis* to respond to environmental stress.

A recent study charactering the genome of *Kingdonia uniflora* (sister to *C. agrestis*) calculated the nucleotide substitution rate of 1.4×10^{-9} per site per year (Sun *et al.*, 2020), which is comparatively lower than an estimate of *Arabidopsis thaliana* (7.0×10^{-9}) (Ossowski *et al.*, 2010) and indirect estimates based on the divergence between monocots and dicots ($5.8\text{-}\ 8.1\times 10^{-9}$) (Wolfe *et al.*, 1987). The low nucleotide substitution rate may be evidence of low speciation rate, which likely contributes to the paucity of species in the family and the low morphological diversity of *C. agrestis* and *K. uniflora*. Low evolution rate is also indicative of low mutation rate, reducing the standing genetic variation which is the genetic source of adaptation (Lai et al., 2019). In isolated populations with high homozygosity and little standing genetic

variation, only large effect alleles can escape the effects of drift becoming the targets of selection (Orr, 1998; Rausher & Delph, 2015; Sella & Barton, 2019). Additionally, many methods for detecting adaptive genetic variation often only have the power to detect loci and alleles with large phenotypic effects (Wellenreuther & Hansson, 2016; Luikart et al., 2018). Nonetheless, genetic patterns that confer adaptation to environmental heterogeneity are mostly polygenic and controlled by numerous genetic variants of small effect (Savolainen *et al.*, 2013; Ahrens *et al.*, 2019). Therefore, the genes identified as putatively adaptive in *C. agrestis* should constitute the first step in studying genetic mechanism of local adaptation in alpine environments. Further work characterizing the whole genome is needed to obtain more precise functions of genes under selective pressure and illuminate patterns of potential polygenic adaptation (Mayol *et al.*, 2019). Generally, these patterns can serve as a proxy for understanding and monitoring the adaptive process in rapidly changing environment (Ahrens *et al.*, 2019), while informing future conservation management.

Conclusions

In this study, we demonstrate two major advances. First, we provide new insights into the genetic structure and evolutionary history of a relictual alpine herb surviving in heterogeneous environment, which can inform further conservation. Our results shed light on vital roles of mountain uplift in promoting population diversification and the dual effect of environmental heterogeneity on species evolutionary history. Second, our analyses provide a roadmap to study evolution of local adaptation of non-model species for which common garden experiments are infeasible and genomic resources are limited. By conducting multiple analyses, we associated environmental variables with genetic variation and explicitly measured the relative influence of bioclimate on population divergence. In turn, the important environmental predictors were implemented in identifying potential loci that may under divergent selection to gain in-depth knowledge of genetic basis involved in local adaptation. More importantly,

our results improve our understanding of drivers and mechanisms of adaptive evolution, aiding efforts on developing sound conservation programs in facing of rapid changing climate.

Acknowledgments

We are grateful to Jie Cai for help with sample collection in Tibet. We thank Jialiang Li and Kangshan Mao for help with the calculation of absolute differentiation (D_{XY}). This work was supported by the Strategic Priority Research Program of Chinese Academy of Sciences (XDA20050203), the Programme Foundation for the Backbone of Scientific Research by Wuhan Botanical Garden, Chinese Academy of Sciences (Y855241G01), the Major Program of National Natural Science Foundation of China (31590823), and the National Key R and D Program of China (2017YFC0505200).

Author contributions

HCW, HS, and YXS developed the idea and designed the experiment. XZ, JWZ, LSY, NL, HJZ, RG, LJL, YHZ and TD collected the leaf materials. XZ and YXS performed the statistical analyses; XZ, YXS, JBL, HS and HCW interpreted the results and wrote the manuscript. All authors read, edited and approved the final manuscript. XZ and YXS contributed equally to this work.

Data accessibility

All newly sequenced plastomes were deposited in National Center for Biotechnology Information (NCBI) with accession numbers MT228704-MT228722. RAD raw read data are stored at the NCBI Sequence Read Archive in the Bioproject PRJNA616150. Genomic data sets and R scripts used in this study are available in the DRYAD archives under accession doi: 10.5061/dryad.4f4qrfj7p.

Reference

Ahrens CW, Byrne M, Rymer PD. 2019. Standing genomic variation within coding and regulatory regions contributes to the adaptive capacity to climate in a foundation tree species. *Mol Ecol* **28**(10): 2502-2516.

Aitken SN, Yeaman S, Holliday JA, Wang T, Curtis-McLane S. 2008. Adaptation, migration or extirpation: climate change outcomes for tree populations. *Evol Appl* **1**(1): 95-111.

Anderson CL, Bremer K, Friis EM. 2005. Dating phylogenetically basal eudicots using *rbcL* sequences and multiple fossil reference points. *American Journal of Botany* **92**: 1737–1748.

Bay RA, Harrigan RJ, Underwood VL, Gibbs HL, Smith TB, Ruegg K. 2018. Genomic signals of selection predict climate-driven population declines in a migratory bird. *Science* **359**(6371): 83.

Bolger AM, Lohse M, Usadel B. 2014. Trimmomatic: a flexible trimmer for Illumina sequence data. *Bioinformatics* **30**(15): 2114-2120.

Bouckaert R, Heled J, Kuhnert D, Vaughan T, Wu CH, Xie D, Suchard MA, Rambaut A, Drummond AJ. 2014. BEAST 2: a software platform for Bayesian evolutionary analysis. *PLoS Comput Biol* **10**(4): e1003537.

Catchen J, Hohenlohe PA, Bassham S, Amores A, Cresko WA. 2013. Stacks: an analysis tool set for population genomics. *Molecular ecology* **22**(11): 3124-3140.

Charlesworth B. 1998. Measures of divergence between populations and the effect of forces that reduce variability. *Molecular Biology and Evolution* **15**: 538–543.

Charlesworth B. 2009. Effective population size and patterns of molecular evolution and variation. *Nature Reviews Genetics* **10**(3): 195-205.

Chen J, Huang Y, Brachi B, Yun Q, Zhang W, Lu W, Li H, Li W, Sun X, Wang G. et al. 2019. Genome-wide analysis of Cushion willow provides insights into alpine plant divergence in a biodiversity hotspot. *Nat Commun* **10**: 5230.

Chen Y-S, Deng T, Zhou Z, Sun H. 2018. Is the East Asian flora ancient or not? *National Science Review* **5**(6): 920-932.

Chung MY, Suh Y, López-Pujol J, Nason JD, Chung MG. 2005. Clonal and fine-scale genetic structure in populations of a restricted Korean endemic, *Hosta jonesii* (Liliaceae) and the implications for conservation. Ann Bot. **96**:279-288.

Colautti RI, Barrett SCH. 2013. Rapid Adaptation to Climate Facilitates Range Expansion of an Invasive Plant. *Science* **342**(6156): 364.

Conover DO, Duffy TA, Hice LA. 2009. The Covariance between Genetic and Environmental Influences across Ecological Gradients. *Annals of the New York Academy of Sciences* **1168**(1): 100-129.

Coop G, Witonsky D, Di Rienzo A, Pritchard JK. 2010. Using Environmental Correlations to Identify Loci Underlying Local Adaptation. *Genetics* **185**(4): 1411.

Coyne JA, Orr HA. 2004. *Speciation*. Sunderland, MA, USA: Sinauer Associates.

Darriba D, Taboada GL, Doallo R, Posada D. 2012. jModelTest 2: more models, new heuristics and parallel computing. *Nat Methods* **9**(8): 772.

Darwin C. 1859. *On the origin of species by means of natural selection, or the preservation of*

favoured races in the struggle for life. London, UK: John Murray.

de Villemereuil P, Gaggiotti OE. 2015. A new FST-based method to uncover local adaptation using environmental variables. *Methods in Ecology and Evolution* **6**(11): 1248-1258.

Deng JY, Fu R-H, Compton SG, Liu M, Wang Q, Yuan C, Zhang L-S, Chen Y. 2020. Sky islands as foci for divergence of fig trees and their pollinators in southwest China. *Mol Ecol.* **29**:762–782.

Dickson BG, Albano CM, Anantharaman R, Beier P, Fargione J, Graves TA, Gray ME, Hall KR, Lawler JJ, Leonard PB, et al. 2019. Circuit-theory applications to connectivity science and conservation. *Conservation Biology* **33**(2): 239-249.

Do C, Waples RS, Peel D, Macbeth GM, Tillett BJ, Ovenden JR. 2014. NeEstimator V2: re-implementation of software for the estimation of contemporary effective population size (*N*e) from genetic data. *Molecular Ecology Resources* **14**(1): 209-214.

Du F, Hou M, Wang W, Mao K, Hampe, A. 2017. Phylogeography of *Quercus aquifolioides* provides novel insights into the Neogene history of a major global hotspot of plant diversity in south-west China. *J. Biogeogr.* **44**: 294-307.

Earl DA, vonHoldt BM. 2012. STRUCTURE HARVESTER: a website and program for visualizing STRUCTURE output and implementing the Evanno method. *Conservation Genetics Resources* **4**(2): 359-361.

Ellegren H. 2014. Genome sequencing and population genomics in non-model organisms. *Trends in Ecology & Evolution* **29**(1): 51-63.

Excoffier L, Laval G, Schneider S. 2007. Arlequin (version 3.0): an integrated software package for population genetics data analysis. *Evolutionary bioinformatics online* **1**: 47-50.

Favre A, Packert M, Pauls SU, Jahnig SC, Uhl D, Michalak I, Muellner-Riehl AN. 2015. The role of the uplift of the Qinghai-Tibetan Plateau for the evolution of Tibetan biotas. *Biol Rev Camb Philos Soc* **90**(1): 236-253.

Fick SE, Hijmans RJ. 2017. WorldClim 2: new 1-km spatial resolution climate surfaces for global land areas. *International Journal of Climatology* **37**(12): 4302-4315.

Forester BR, Lasky JR, Wagner HH, Urban DL. 2018. Comparing methods for detecting multilocus adaptation with multivariate genotype–environment associations. *Molecular Ecology* **27**(9): 2215-2233.

Foster AS. 1971. Additional studies on the morphology of blind vein-endings in the leaf of circaeaster agrestis. *American Journal of Botany* **58**(3): 263-272.

Frichot E & Francois O. 2015. LEA: an R package for Landscape and Ecological Association studies. *Methods in Ecology and Evolution* **6**:925-929.

Frichot E, Mathieu F, Trouillon T, Bouchard G, Francois O. 2014. Fast and efficient estimation of individual ancestry coefficients. *Genetics* **196**:973-983.

Friis G, Fandos G, Zellmer AJ, McCormack JE, Faircloth BC, Milá B. 2018. Genome-wide signals of drift and local adaptation during rapid lineage divergence in a songbird. *Molecular Ecology* **27**(24): 5137-5153.

Fu D, Bartholomew B 2001. CIRCAEASTERACEAE. In: Wu ZY, Raven, P. H. & Hong, D. Y. ed. *Flora of China*. Beijing & St. Louis: Science Press & Missouri Botanical Garden

Press, 439.

Gao LM, MÖLler M, Zhang XM, Hollingsworth ML, Liu J, Mill RR, Gibby M, Li DZ. 2007. High variation and strong phylogeographic pattern among cpDNA haplotypes in *Taxus wallichiana* (Taxaceae) in China and North Vietnam. *Molecular Ecology* **16**(22): 4684-4698.

Goicoechea PG, Guillardín L, Fernández-Ibarrodo L, Valbuena-Carabaña M, González-Martínez SC, Alía R, Kremer A. 2019. Adaptive Introgression Promotes Fast Adaptation In Oaks Marginal Populations. *bioRxiv*: 731919.

Gotz S, Garcia-Gomez JM, Terol J, Williams TD, Nagaraj SH, Nueda MJ, Robles M, Talon M, Dopazo J, Conesa A. 2008. High-throughput functional annotation and data mining with the Blast2GO suite. *Nucleic Acids Res* **36**(10): 3420-3435.

Goudet J, Raymond M, de Meeüs T, Rousset F. 1996. Testing Differentiation in Diploid Populations. *Genetics* **144**(4): 1933.

Gu Y, Kaplinsky N, Bringmann M, Cobb A, Carroll A, Sampathkumar A, Baskin TI, Persson S, Somerville CR. 2010. Identification of a cellulose synthase-associated protein required for cellulose biosynthesis. *Proceedings of the National Academy of Sciences* **107**(29): 12866.

Gugger PF, Liang CT, Sork VL, Hodgskiss P, Wright JW. 2017. Applying landscape genomic tools to forest management and restoration of Hawaiian koa (*Acacia koa*) in a changing environment. *Evolutionary Applications* **11**(2): 231-242.

He K, Jiang XL. 2014. Sky islands of southwest China. I: An overview of phylogeographic patterns. *Chinese Science Bulletin* **59**: 585-597.

Heled J. 2010. Extended Bayesian Skyline Plots Tutorial.

Heled J, Drummond AJ. 2008. Bayesian inference of population size history from multiple loci. *BMC Evolutionary Biology* **8**(1): 289.

Hill WG. 1981. Estimation of effective population size from data on linkage disequilibrium. *Genetical Research* **38**:209-216.

Ho SYW, Phillips MJ. 2009. Accounting for Calibration Uncertainty in Phylogenetic Estimation of Evolutionary Divergence Times. *Systematic Biology* **58**(3): 367-380.

Hoban S, Kelley JL, Lotterhos KE, Antolin MF, Bradburd G, Lowry DB, Poss ML, Reed LK, Storfer A, Whitlock MC. 2016. Finding the Genomic Basis of Local Adaptation: Pitfalls, Practical Solutions, and Future Directions. *The American Naturalist* **188**(4): 379-397.

Hughes AC. 2017. Understanding the drivers of Southeast Asian biodiversity loss. *Ecosphere*, **8**(1): e01624.

Hughes CE & Atchison GW. 2015. The ubiquity of alpine plant radiations: from the Andes to the Hengduan Mountains. *New Phytol.* 207: 275-282.

Jakobsson M, Rosenberg NA. 2007. CLUMPP: a cluster matching and permutation program for dealing with label switching and multimodality in analysis of population structure. *Bioinformatics* **23**(14): 1801-1806.

Janes JK, Miller JM, Dupuis JR, Malenfant RM, Gorrell JC, Cullingham CI. 2017. The *K*

= 2 conundrum. *Mol Ecol.* **26**: 3594-3602.

Jia K-H, Zhao W, Maier PA, Hu X-G, Jin Y, Zhou S-S, Jiao S-Q, El-Kassaby YA, Wang T, Wang X-R, et al. 2019. Landscape genomics predicts climate change-related genetic offset for the widespread *Platycladus orientalis* (Cupressaceae). *Evolutionary Applications* https://doi.org/10.1111/eva.12891.

Jiang X-L, Gardner EM, Meng H-H, Deng M, Xu G-B. 2019. Land bridges in the Pleistocene contributed to flora assembly on the continental islands of South China: Insights from the evolutionary history of *Quercus championii*. *Molecular Phylogenetics and Evolution* **132**: 36-45.

Jombart T. 2008. adegenet: a R package for the multivariate analysis of genetic markers. *Bioinformatics* **24**(11): 1403-1405.

Katoh K, Standley DM. 2013. MAFFT multiple sequence alignment software version 7: improvements in performance and usability. *Mol Biol Evol* **30**(4): 772-780.

Kawecki TJ, Ebert D. 2004. Conceptual issues in local adaptation. *Ecology Letters* **7**(12): 1225-1241.

Kearse M, Moir R, Wilson A, Stones-Havas S, Cheung M, Sturrock S, Buxton S, Cooper A, Markowitz S, Duran C, et al. 2012. Geneious Basic: an integrated and extendable desktop software platform for the organization and analysis of sequence data. *Bioinformatics* **28**(12): 1647-1649.

Kimura M, Crow JF. 1964. The number of alleles that can be maintained in a finite population. *Genetics* **49**(4): 725-738.

Kramer AT, Havens K. 2009. Plant conservation genetics in a changing world. *Trends in Plant Science* **14**(11): 599-607.

Lai Y, Yeung KL, Omland E, Pang EL, Liao BY, Cao HF, Zhang BW, Yeh CF, Hung CM, Hung HY, et al. 2019. Standing genetic variation as the predominant source for adaptation of a songbird. *Proc Natl Acad Sci USA* **116:** 2152-2157.

Li H, Luan S. 2011. The cyclophilin AtCYP71 interacts with CAF-1 and LHP1 and functions in multiple chromatin remodeling processes. *Mol Plant* **4**(4): 748-758.

Li J, Milne RI, Ru D, Miao J, Tao W, Zhang L, Xu J, Liu J, Mao K. 2020. Allopatric divergence and hybridization within *Cupressus chengiana* (Cupressaceae), a threatened conifer in the northern Hengduan Mountains of western China. *Molecular Ecology* doi:10.1111/mec.15407.

Li Y, Zhai S-N, Qiu Y-X, Guo Y-P, Ge X-J, Comes HP. 2011. Glacial survival east and west of the 'Mekong–Salween Divide'in the Himalaya–Hengduan Mountains region as revealed by AFLPs and cpDNA sequence variation in *Sinopodophyllum hexandrum* (Berberidaceae). *Molecular Phylogenetics and Evolution* **59**(2): 412-424.

Lin N, Deng T, Moore MJ, Sun Y, Huang X, Sun W, Luo D, Wang H, Zhang J, Sun H. 2018. Phylogeography of *Parasyncalathium souliei* (Asteraceae) and Its Potential Application in Delimiting Phylogeoregions in the Qinghai-Tibet Plateau (QTP)-Hengduan Mountains (HDM) Hotspot. *Front. Genet.* **9**:171.

Liu J, Möller M, Provan J, Gao L-M, Poudel RC, Li D-Z. 2013. Geological and ecological factors drive cryptic speciation of yews in a biodiversity hotspot. *New Phytologist*

199(4): 1093-1108.

Lowry DB, Lovell JT, Zhang L, Bonnette J, Fay PA, Mitchell RB, Lloyd-Reilley J, Boe AR, Wu Y, Rouquette FM, et al. 2019. QTL × environment interactions underlie adaptive divergence in switchgrass across a large latitudinal gradient. *Proceedings of the National Academy of Sciences* **116**(26): 12933.

Lu HY & Guo ZT. 2014. Evolution of the monsoon and dry climate in East Asia during late Cenozoic: a review. *Science China Earth Sciences* **57**: 70–79.

Luikart G, Kardos M, Hand BK, Rajora OP, Aitken SN, Hohenlohe PA. 2018. Population genomics: advancing understanding of nature. In: Rajora OP, ed. *Population genomics: concepts, approaches and applications.* Cham, Switzerland: Springer, 3–79.

Mayol M, Riba M, Cavers S, Grivet D, Vincenot L, Cattonaro F, Vendramin G, González□Martínez SC. 2019. A multiscale approach to detect selection in nonmodel tree species: Widespread adaptation despite population decline in *Taxus baccata* L. *Evol Appl.***00**:1–18.

McCormack JE, Hird SM, Zellmer AJ, Carstens BC, Brumfield RT. 2013. Applications of next-generation sequencing to phylogeography and phylogenetics. *Molecular Phylogenetics and Evolution* **66**(2): 526-538.

McRae BH. 2006. Isolation by resistance. *Evolution* **60**:1551–1561.

McRae BH, Dickson BG, Keitt TH, Shah VB. 2008. Using circuit theory to model connectivity in ecology, evolution, and conservation. *Ecology* **89**:2712–2724.

Mulch A & Chamberlain CP. 2006. Earth science – The rise and growth of Tibet. *Nature* **439**: 670–671.

Mustilli AC, Merlot S, Vavasseur A, Fenzi F, Giraudat J. 2002. Arabidopsis OST1 protein kinase mediates the regulation of stomatal aperture by abscisic acid and acts upstream of reactive oxygen species production. *The Plant cell* **14**(12): 3089-3099.

Myers N, Mittermeier RA, Mittermeier CG, da Fonseca GA, Kent J. 2000. Biodiversity hotspots for conservation priorities. *Nature* 403: 853–858.

Nevado B, Wong ELY, Osborne OG, Filatov DA. 2019. Adaptive Evolution Is Common in Rapid Evolutionary Radiations. *Current Biology* **29**: 3081–3086.

Noroozi J, Talebi A, Doostmohammadi M, Rumpf SB, Linder HP, Schneeweiss GM. 2018. Hotspots within a global biodiversity hotspot – Areas of endemism are associated with high mountain ranges. *Scientific Reports* **8**: 10345

Nowakowski AJ, DeWoody JA, Fagan ME, Willoughby JR, Donnelly MA. 2015. Mechanistic insights into landscape genetic structure of two tropical amphibians using field-derived resistance surfaces. *Mol Ecol* **24**(3): 580-595.

Oakley CG & Winn AA. 2012. Effects of population size and isolation on heterosis, mean fitness, and inbreeding depression in a perennial plant. *New Phytologist* **196**: 261-270.

Oksanen J, Blanchet FG, Friendly M, Kindt R, Legendre P, McGlinn D, Minchin PR, O'Hara RB, Simpson GL, Solymos P, et al. 2018. Vegan: Community Ecology Package. https://CRAN.R-project.org/package=vegan.

Orr HA. 1998. The population genetics of adaptation: the distribution of factors fixed during adaptive evolution. *Evolution* 52:935-949.

Ossowski S, Schneeberger K, Lucas-Lledo JI, Warthmann N, Clark RM, et al. 2010. The rate and molecular spectrum of spontaneous mutations in *Arabidopsis thaliana*. *Science* **327**:92-94

Peakall R, Smouse PE. 2012. GenAlEx 6.5: genetic analysis in Excel. Population genetic software for teaching and research--an update. *Bioinformatics* **28**(19): 2537-2539.

Pham J, Liu J, Bennett MH, Mansfield JW, Desikan R. 2012. Arabidopsis histidine kinase 5 regulates salt sensitivity and resistance against bacterial and fungal infection. *New Phytol* **194**(1): 168-180.

Phillips SJ, Dudik M. 2008. Modeling of species distributions with Maxent: new extensions and a comprehensive evaluation. *Ecography* **31**(2): 161-175.

Plummer M, Best N, Cowles K, Vines K. 2006. CODA: convergence diagnosis and output analysis for MCMC. *R News* **6**(1): 7-11.

Poudel RC, Möller M, Liu J, Gao L-M, Baral SR, Li D-Z. 2014. Low genetic diversity and high inbreeding of the endangered yews in Central Himalaya: implications for conservation of their highly fragmented populations. *Diversity and Distributions* **20**(11): 1270-1284.

Pritchard JK, Stephens M, Donnelly P. 2000. Inference of population structure using multilocus genotype data. *Genetics* **155**(2): 945-959.

Qu XJ, Moore MJ, Li DZ, Yi TS. 2019. PGA: a software package for rapid, accurate, and flexible batch annotation of plastomes. *Plant Methods* **15**(1): 50.

R Team C 2014. R: A language and environment for statistical computing. R Foundation for Statistical Computing. Vienna, Austria.

Rambaut A, Drummond A. 2010. TreeAnnotator version 1.6. 1. *University of Edinburgh, Edinburgh, UK.* Available at: http://beast.bio.ed.ac.uk.

Rambaut A, Drummond AJ, Xie D, Baele G, Suchard MA. 2018. Posterior Summarization in Bayesian Phylogenetics Using Tracer 1.7. *Syst Biol* **67**(5): 901-904.

Rausher MD & Delph LF. 2015. Commentary: When does understanding phenotypic evolution require identification of the underlying genes? *Evolution* **69**(7): 1655–1664.

Ree RH, Sanmartín I. 2009. Prospects and challenges for parametric models in historical biogeographical inference. *Journal of Biogeography* **36**: 1211-1220.

Rellstab C, Gugerli F, Eckert AJ, Hancock AM, Holderegger R. 2015. A practical guide to environmental association analysis in landscape genomics. *Molecular Ecology* **24**(17): 4348-4370.

Ren G, Mateo RG, Liu J, Suchan T, Alvarez N, Guisan A, Conti E, Salamin N. 2017. Genetic consequences of Quaternary climatic oscillations in the Himalayas: *Primula tibetica* as a case study based on restriction site-associated DNA sequencing. *New Phytologist* **213**(3): 1500-1512.

Ren Y, Li Z, Hu Z. 2003. Approaches to the systematic position of *Circaeaster* based on the morphological data. *Acta Botanica Boreali-occidentalia Sinica* **23**(7): 1091-1097.

Rochette NC, Catchen JM. 2017. Deriving genotypes from RAD-seq short-read data using Stacks. *Nature Protocols* **12**: 2640.

Rosenberg NA. 2004. Distruct: a program for the graphical display of population structure.

Molecular Ecology Notes **4**(1): 137-138.

Rozas J, Ferrer-Mata A, Sanchez-DelBarrio JC, Guirao-Rico S, Librado P, Ramos-Onsins SE, Sanchez-Gracia A. 2017. DnaSP 6: DNA Sequence Polymorphism Analysis of Large Data Sets. *Mol Biol Evol* **34**(12): 3299-3302.

Ru D, Sun Y, Wang D, Chen Y, Wang T, Hu Q, Abbott RJ, Liu J. 2018. Population genomic analysis reveals that homoploid hybrid speciation can be a lengthy process. *Molecular Ecology* **27**(23): 4875-4887.

Ruiz-Sanchez E, Rodriguez-Gomez F, Sosa V. 2012. Refugia and geographic barriers of populations of the desert poppy, *Hunnemannia fumariifolia* (Papaveraceae). *Organisms Diversity & Evolution* **12**(2): 133-143.

Savolainen O, Lascoux M, Merilä J. 2013. Ecological genomics of local adaptation. *Nature Reviews Genetics* **14**: 807.

Savolainen O, Pyhäjärvi T, Knürr T. 2007. Gene Flow and Local Adaptation in Trees. *Annual Review of Ecology, Evolution, and Systematics* **38**(1): 595-619.

Seehausen O, Butlin RK, Keller I, Wagner CE, Boughman JW, Hohenlohe PA, Peichel CL, Saetre G-P, Bank C, Brännström Å, et al. 2014. Genomics and the origin of species. *Nature Reviews Genetics* **15**: 176.

Sella G & Barton NH. 2019. Thinking About the Evolution of Complex Traits in the Era of Genome-Wide Association Studies. *Annu. Rev. Genom. Hum. Genet*. **20**:461-93

Sierla M, Horak H, Overmyer K, Waszczak C, Yarmolinsky D, Maierhofer T, Vainonen JP, Salojarvi J, Denessiouk K, Laanemets K, et al. 2018. The Receptor-like Pseudokinase GHR1 Is Required for Stomatal Closure. *The Plant cell* **30**(11): 2813-2837.

Song JH, Kang HS, Byun YH, Hong SY. 2010. Effects of the Tibetan Plateau on the Asian summer monsoon: a numerical case study using a regional climate model. *International Journal of Climatology* 30: 743–759.

Spieth PT. 1974. Gene flow and genetic differentiation. *Genetics* **78**(3): 961.

Stroud DA, Surgenor EE, Formosa LE, Reljic B, Frazier AE, Dibley MG, Osellame LD, Stait T, Beilharz TH, Thorburn DR, et al. 2016. Accessory subunits are integral for assembly and function of human mitochondrial complex I. *Nature* **538**(7623): 123-126.

Sun B-N, Wu J-Y, Liu Y-S, Ding S-T, Li X-C, Xie S-P, Yan D-F, Lin Z-C. 2011. Reconstructing Neogene vegetation and climates to infer tectonic uplift in western Yunnan, China. *Palaeogeography, Palaeoclimatology, Palaeoecology* **304**(3): 328-336.

Sun H, Zhang J, Deng T, Boufford DE. 2017. Origins and evolution of plant diversity in the Hengduan Mountains, China. *Plant Diversity* **39**(4): 161-166.

Sun Y, Moore MJ, Landis JB, Lin N, Chen L, Deng T, Zhang J W., Meng AP, Zhang SJ, Tojibaev OS, et al. (2018). Plastome phylogenomics of the early-diverging eudicot family Berberidaceae. *Mol. Phylogenet. Evol.* **128**: 203–211.

Sun Y, Deng T, Zhang A, Moore MJ, Landis JB, Lin N, Zhang H, Zhang X, Huang J, Zhang X, et al. 2020. The draft genome of the endangered, relictual plant *Kingdonia uniflora* (Circaeasteraceae, Ranunculales) reveals potential mechanisms and perils of

evolutionary specialization. *bioRxiv*: 2020.2001.2008.898460.

Sun Y, Moore MJ, Lin N, Adelalu KF, Meng A, Jian S, Yang L, Li J, Wang H. 2017. Complete plastome sequencing of both living species of Circaeasteraceae (Ranunculales) reveals unusual rearrangements and the loss of the *ndh* gene family. *BMC Genomics* **18**(1): 592.

Tang H, Micheels A, Eronen JT, Ahrens B & Fortelius M. 2013. Asynchronous responses of East Asian and Indian summer monsoons to mountain uplift shown by regional climate modelling experiments. *Climate Dynamics* **40**: 1531–1549.

Tognetti VB, Van Aken O, Morreel K, Vandenbroucke K, van de Cotte B, De Clercq I, et al. 2010. Perturbation of indole-3-butyric acid homeostasis by the UDP-glucosyltransferase UGT74E2 modulates Arabidopsis architecture and water stress tolerance. *The Plant cell*, **22**(8), 2660-2679.

von Balthazar M, Pedersen K, Friis E. 2005. *Teixeiraea lusitanica*, a new fossil flower from the Early Cretaceous of Portugal with affinities to the Ranunculales. *Plant Systematics and Evolution* **255**: 55–75.

Wang J, Santiago E, Caballero A. 2016. Prediction and estimation of effective population size. *Heredity* **117**: 193-206.

Waples RS. 2006. A bias correction for estimates of effective population size based on linkage disequilibrium at unlinked gene loci. *Conservation Genetics* **7**:167-184.

Weigel D, Nordborg M. 2015. Population Genomics for Understanding Adaptation in Wild Plant Species. *Annual Review of Genetics* **49**(1): 315-338.

Weir BS, Cockerham CC. 1984. Estimating F-statistics for the analysis of population structure. *Evolution* **38**(6): 1358-1370.

Wellenreuther M, Hansson B. 2016. Detecting polygenic evolution: problems, pitfalls, and promises. *Trends Genet.* **32**:155–64.

Wen J, Zhang JQ, Nie ZL, Zhong Y, Sun H. 2014. Evolutionary diversifications of plants on the Qinghai-Tibetan Plateau. *Front Genet* **5**: 4.

Wolfe KH, Li WH, Sharp PM. 1987. Rates of nucleotide substitution vary greatly among plant mitochondrial, chloroplast, and nuclear DNAs. *Proc Natl Acad Sci USA* **84**: 9054-9058.

Wright S. 1946. Isolation by distance under diverse systems of mating. *Genetics* **31**(1): 39-59.

Wu ZY, Wu SG. 1996. A proposal for a new floristic kingdom (realm): the E. Asiatic Kingdom, its delineation and characteristics. In: Zhang AL, Wu SG, eds. *Floristic characteristics and diversity of East Asian plants*. Beijing, China: China Higher Education Press/Springer, 3–42.

Yang JB, Li DZ, Li HT. 2014. Highly effective sequencing whole chloroplast genomes of angiosperms by nine novel universal primer pairs. *Mol Ecol Resour* **14**(5): 1024-1031.

Yang ZY, Yi TS, Pan YZ Gong X. 2012. Phylogeography of an alpine plant *Ligularia vellerea* (Asteraceae) in the Hengduan Mountains. *J Syst Evol* **50**:316–324

Yu Y, Harris AJ, Blair C, He X. 2015. RASP (Reconstruct Ancestral State in Phylogenies): a tool for historical biogeography. *Mol Phylogenet Evol* **87**: 46-49.

Zhang D, Gao F, Jakovlic I, Zou H, Zhang J, Li WX, Wang GT. 2019. PhyloSuite: An

integrated and scalable desktop platform for streamlined molecular sequence data management and evolutionary phylogenetics studies. *Mol Ecol Resour* doi:10.1111/1755-0998.13096.

Table 1 Summary of statistics calculated for the 6120 variant positions. n, number of genotype; π, average nucleotide diversity; H_e, average expected heterozygosity per locus; H_o, average observed heterozygosity per locus; the inbreeding coefficients (F_{IS}). The statistics of six defined groups are bolded. E1, eastern group1; E2, eastern group2; W1, western group1; W2, western group2; W3, western group3; W4, western group4

Group IDs	Population IDs	n	π	H_e	H_o	F_{IS}
E1	**-**	**75**	**0.0464**	**0.0461**	**0.0029**	**0.1952**
	SNJ	13	0.0207	0.0199	0.0038	0.0383
	TBS	17	0.0218	0.0212	0.0029	0.0532
	HZ2	9	0.0008	0.0007	0.0014	-0.0010
	HZ3	10	0.0013	0.0012	0.0022	-0.0017
	KMG	8	0.0015	0.0014	0.0027	-0.0023
	TSM	9	0.0214	0.0203	0.0027	0.0425
	WLG	4	0.0306	0.0287	0.0034	0.0621
	XLS	5	0.0223	0.0210	0.0026	0.0375
E2	**-**	**19**	**0.0384**	**0.0374**	**0.0034**	**0.1011**
	BLS	9	0.0216	0.0204	0.0035	0.0529
	SGN	10	0.0254	0.0241	0.0033	0.0573
W1	**-**	**7**	**0.0688**	**0.0639**	**0.0548**	**0.0384**
	MXG	4	0.0215	0.0189	0.0220	-0.0005
	YL	1	0.0016	0.0008	0.0016	-
	ZG	2	0.1633	0.1225	0.1470	0.0244
W2	**DDL**	**9**	**0.1646**	**0.1555**	**0.2650**	**-0.1806**
W3	**SJL**	**10**	**0.0206**	**0.0196**	**0.0134**	**0.0227**
W4	**-**	**19**	**0.0249**	**0.0242**	**0.0088**	**0.0510**
	YH	8	0.0150	0.0140	0.0057	0.0238
	GS	1	0.0255	0.0128	0.0255	-
	ZF	10	0.0136	0.0130	0.0095	0.0100

Table 2 RDA results based on six important environmental variables identified by GF analysis.

Environmental variables	Constrained proportion	*F*	*p*
Bio03	0.1893	31.98	0.001**
AET	0.1712	28.31	0.001**
Bio04	0.1408	22.45	0.001**
Bio12	0.0902	13.59	0.001**
Bio07	0.0627	9.17	0.001**
Bio15	0.0203	2.84	0.001**

Table 3 Annotation information of 16 candidate loci under selection that the E-value of blastx is less than 1E-5. Detailed functional annotation is provided in Table S11.

Loci ID	Gene names	Description	Length	E-Value	Similarity
2763	*UGT74E2*	UDP-glycosyltransferase 74E2-like	146	1.16E-19	82.08
8038	*SRK2E*	Serine/threonine-protein kinase TIO-like isoform X1	146	4.97E-07	81.56
8150	*CSC1*	Calcium permeable stress-gated cation channel 1-like	146	5.12E-20	92.71
19591	*At1g18270*	Ketose-bisphosphate aldolase class-II family protein	146	6.34E-06	87.07
83859	*NDUFS7*	NADH dehydrogenase subunit 7 (mitochondrion)	146	7.55E-26	93.96
126986	*RTL*	Retrotransposon gag protein	147	4.78E-14	84.5
146932	*RPPL1*	Putative disease resistance RPP13-like protein 1 isoform X1	146	2.78E-06	87.52
203056	*AHK5*	Histidine kinase 5	146	7.55E-14	84.61
206146	*ABCC2*	ABC transporter C family member 2-like	146	2.77E-15	89.16
218068	*CSI1*	Protein cellulose synthase interactive 1	146	3.74E-14	86.88
219291	*NDUFB3*	NADH dehydrogenase [ubiquinone] 1 beta subcomplex subunit 3-B-like	146	8.26E-20	82.13
243120	*NUDT8*	Nudix hydrolase 8	146	8.49E-14	81.72
275249	*N/A*	Glycosyl transferase (glycosyl transferase family 2)	146	3.38E-24	85.59
293398	*CYP71*	Peptidyl-prolyl cis-trans isomerase CYP71	146	7.81E-17	92.11
296907	*N/A*	Glucan endo-1,3-beta-glucosidase 13-like	146	1.45E-20	83.33
305334	*CSLC6*	Probable xyloglucan glycosyltransferase 6	146	7.31E-26	98.54

Figure legends

Fig. 1 Geographical distribution of haplotypes detected in polymorphic sites of *Circaeaster agrestis* populations. Colors indicate genetic groups based on STRUCTURE and PoCA results (see also Fig. 2), with the Eastern clade being made up of the orange and dark green circles, with the Western clade consisting of the light green, light pink, purple, and blue circles. Circle sizes reflect the number of individuals sampled.

Fig. 2 Population genetic structure in *Circaeaster agrestis* based on 6,120 SNPs from (a) PCoA for all populations, east-clade and west-clade, corresponding percentage of variation explained by each principal component is provided in **Fig. S5**; and (b) STRUCTURE with K=2 (showing the highest ΔK; Fig. S4a) and 6 (representing the divergence within east and west clades).

Fig. 3 Evolutionary history of *Circaeaster agrestis*. (a) Divergent time estimation and ancestral area reconstructions of 66 haplotypes using BEAST and statistical dispersal-extinction-cladogenesis (S-DEC), respectively. Mean divergence dates and 95% HPDs for major nodes (1–5) are summarized in top left. Pie charts on each node indicate marginal probabilities for each alternative ancestral area derived from S-DEC. Results are based on a maximum area number of two. Inferred dispersal and vicariance events are indicated by green and red circle respectively. (b) Five biogeographic regions representing the current distributions of *C. agrestis*, according to the floristic division of China proposed by Wu & Wu (1998) and the study of Lin et al., (2018): A, Qinling-Daba Mountains; B, North Hengduan Mountains; C, North QTP; D, South Hengduan Mountains; E, East Himalayan regions. (c) Temporal changes in the effective population size (N_e) changes inferred with Extended Bayesian skyline plots (EBSP) using BEAST2. Re, reproductive number, δ, death rate.

Fig. 4 Topographic and ecological effects on genetic structure. Relationship of genetic distance and (a) geographical distance, (b) resistance distance based on climatic niche suitability, as tested by a Mantel test. (c) Conductance grid derived from the Isolation-

by-Resistance (IBR) model. Grid with warm colour indicates high conductance, cold colour indicates high resistance.

Fig. 5 (a) R2-weighted importance of environmental variables that explain genetic gradients from gradient forest (GF) analysis. (b) Cumulative importance of allelic change along the first six environmental gradients. The units of environmental variables are provided in the parentheses. SD, standard deviation.

Fig. 6 Redundancy analysis showing the relationship between the independent climate parameters and population structure. Individuals are colored points and colors represent six groups (E1, E2, W1, W2, W3, W4). Small black points are SNPs. The definition of each climate variable is provided in the top right corner.

Supporting information

Fig. S1 The known distribution area of the Circaeaster agrestis based on all recorded sampling points available in Chinese Virtual Herbarium (CVH; http://www.cvh.ac.cn/). The green triangles indicate sampling locations in this study. The red cross indicates a distribution record in reported in 1997, but not available now based on one recent field investigation in 2018.

Fig. S2 (a) The number of 80% polymorphic loci shared across most samples (the r80 loci) as M=n increases. (b) The distribution of the number of SNPs per locus for a range of M=n values.

Fig. S3 (a) F_{ST} values within populations estimated by *hierfstat*, Group names of populations were labeled in the top of boxes. (b) F_{ST} values within genetic groups estimated by *hierfstat.* (c) The results of G-statistic test.

Fig. S4 The optimal *K* value identified using (a) delta-*K* method in STRUCTURE HARVESTER, and (b) cross-entropy criterion in R package *LEA.*

Fig. S5 Scree plot of the percentage of variation explained by each principal component (PC), corresponding to **Fig. 2a** for all populations, East-clade and West-clade, respectively.

Fig. S6 Divergence times of Ranunculales estimated by BEAST2 with a relaxed molecular clock based on the combined protein-coding region sequences. A and B indicate fossil calibration points. C and D indicate the origination and diversification of Circaeaster agrestis, respectively. Median ages of nodes are shown with bars indicating the 95% highest posterior density intervals for each node.

Fig. S7 Ancestral area reconstructions of 66 haplotypes using statistical dispersal vicariance (S-DIVA) analysis. Pie charts on each node indicate marginal probabilities for each alternative ancestral area derived from S-DIVA. Results are based on a maximum area number of two. Inferred dispersal and vicariance events are indicated by green and red circle respectively. Defined biogeographic regions are the same as the statistical dispersal-extinction-cladogenesis analysis (Fig. 3).

Table S1 Summary of population information of *Circaeaster agrestis*, including the number of individuals genotyped at each localities (n), geographic information,voucher specimens information, and 20 bioclimate values (bio01-bio19 and AET) of each location. AET, the actual evapotranspiration. The units of environmental variables are provided in the parentheses. SD, standard deviation.

Table S2 Numbers of reads of RAD-seq for each individual of *Circaeaster agrestis*.

Table S3 Assemble and annotation information of newly sequenced plastomes of *Circaeaster agrestis* populations.

Table S4 Summary of statistics calculated for the 22915 variant positions. n, number of genotype; π, average nucleotide diversity; He, average expected heterozygosity per locus; Ho, average observed heterozygosity per locus; the inbreeding coefficients (FIS). The statistics of six defined groups are bolded. E1, eastern group1; E2, eastern group2; W1, western group1; W2, western group2; W3, western group3; W4, western group4.

Table S5 Haplotypes information detected in 18 populations based on 6120 SNPs.

Table S6 Paired population-level FST estimated by *hierfstat* using Weir and Cockerham's method.

Table S7 Estimated Ne values using linkage disequilibrium method, implemented in

NeEstimator, with a minor allele frequency cutoff of 0.05 and 95% confidence intervals (CI) estimated by jackknifing. The statistics of six defined groups are bolded. E1, eastern group1; E2, eastern group2; W1, western group1; W2, western group2; W3, western group3; W4, western group4; n, number of genotype.

Table S8 The analysis of molecular variance (AMOVA) for SNP data among six genetic groups (E1, E2, W1, W2, W3 and W4)

Table S9 Paired group-level FST estimated by *hierfstat* using Weir and Cockerham's method.

Table S10 Paired mean absolute differentiation (D_{XY}) among genetic groups using a Perl script provided by Ru et al., (2018).

Table S11 Detailed annotation information of sixteen genes under potential divergent selection. GO: Gene Ontology

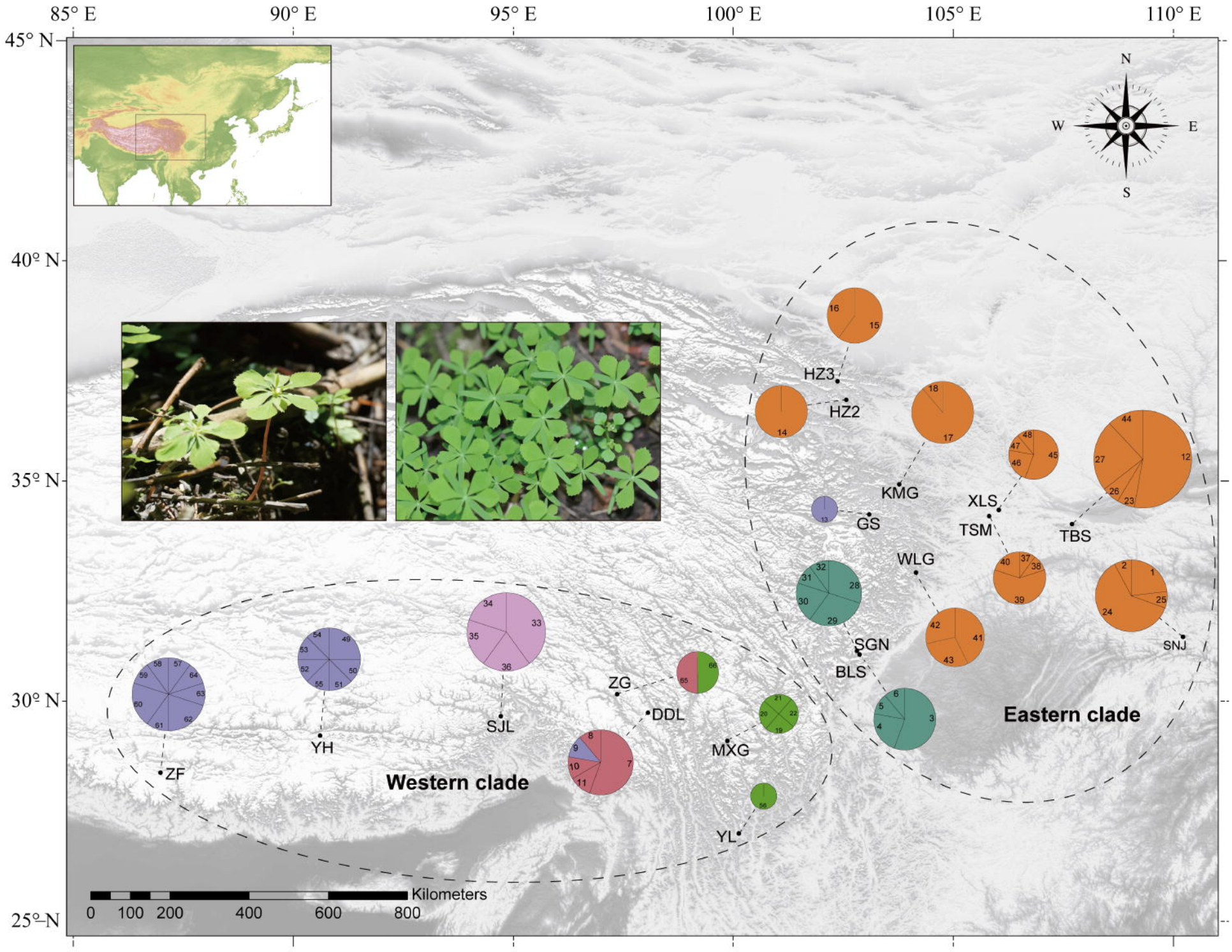
85° E
90° E
95° E
100° E
105° E
110° E
45° N
40° N
35° N
30° N
25° N
N
S
W
E
HZ3
HZ2
KMG
GS
XLS
TSM
TBS
WLG
SGN
BLS
SNJ
ZG
DDL
SJL
YH
ZF
MXG
YL
Eastern clade
Western clade
Kilometers
0 100 200 400 600 800

(a)

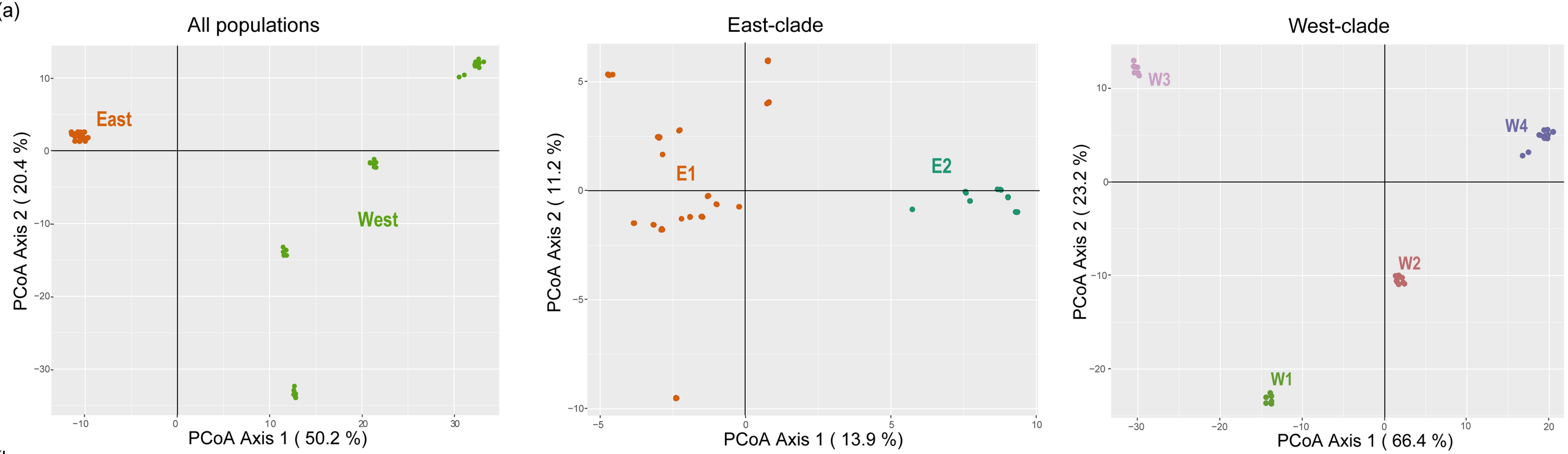
All populations
East
West
PCoA Axis 2 (20.4 %)
PCoA Axis 1 (50.2 %)
East-clade
E1
E2
PCoA Axis 2 (11.2 %)
PCoA Axis 1 (13.9 %)
West-clade
W3
W4
W2
W1
PCoA Axis 2 (23.2 %)
PCoA Axis 1 (66.4 %)

(b)

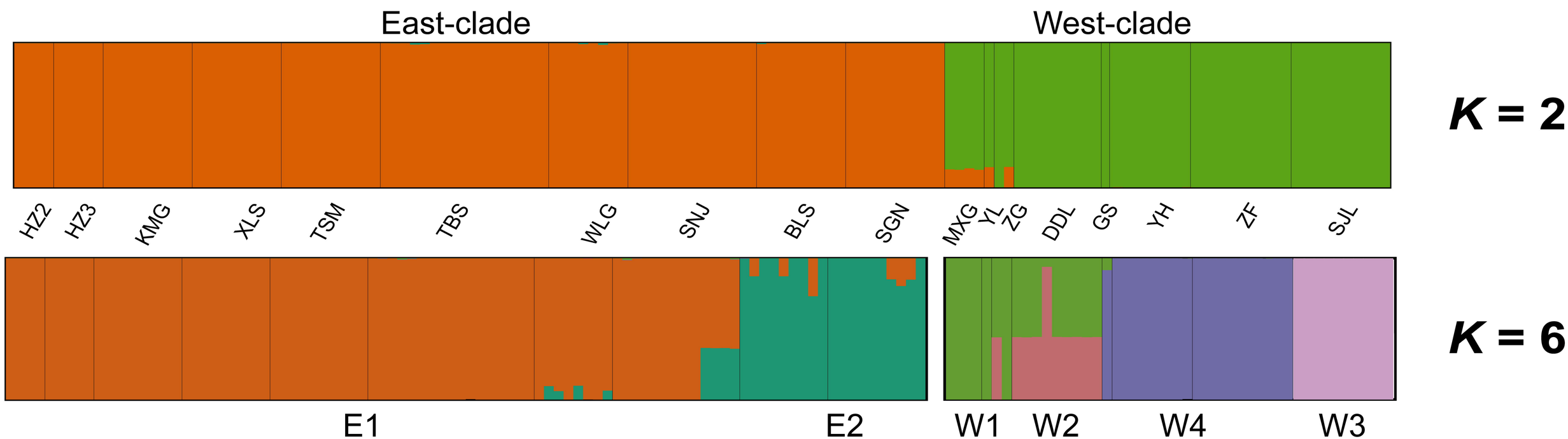
East-clade
West-clade
K = 2
HZ2
HZ3
KMG
XLS
TSM
TBS
WLG
SNJ
BLS
SGN
MXG
YL
ZG
DDL
GS
YH
ZF
SJL
K = 6
E1
E2
W1
W2
W4
W3

(a)

Node	Time	95% HPD
1	6.71	5.18-7.98
2	5.03	3.45-7.49
3	3.96	2.63-5.04
4	3.77	2.50-4.90
5	2.90	1.71-4.37

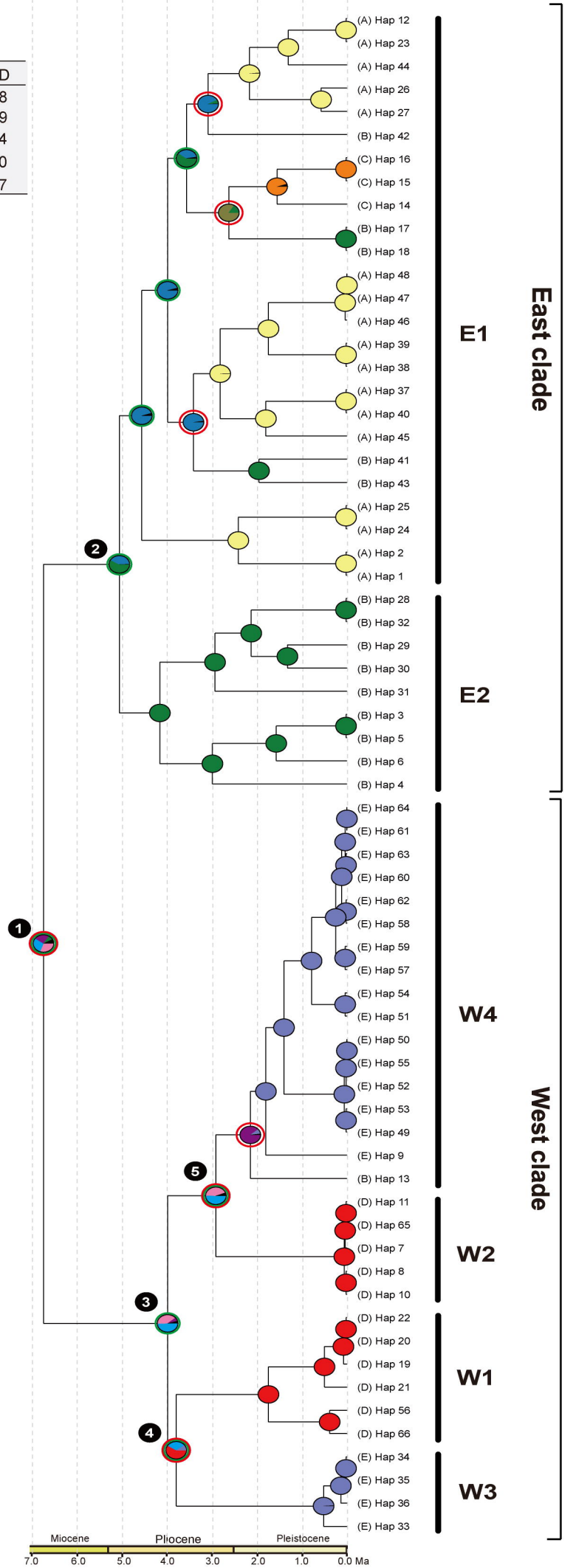

(b)

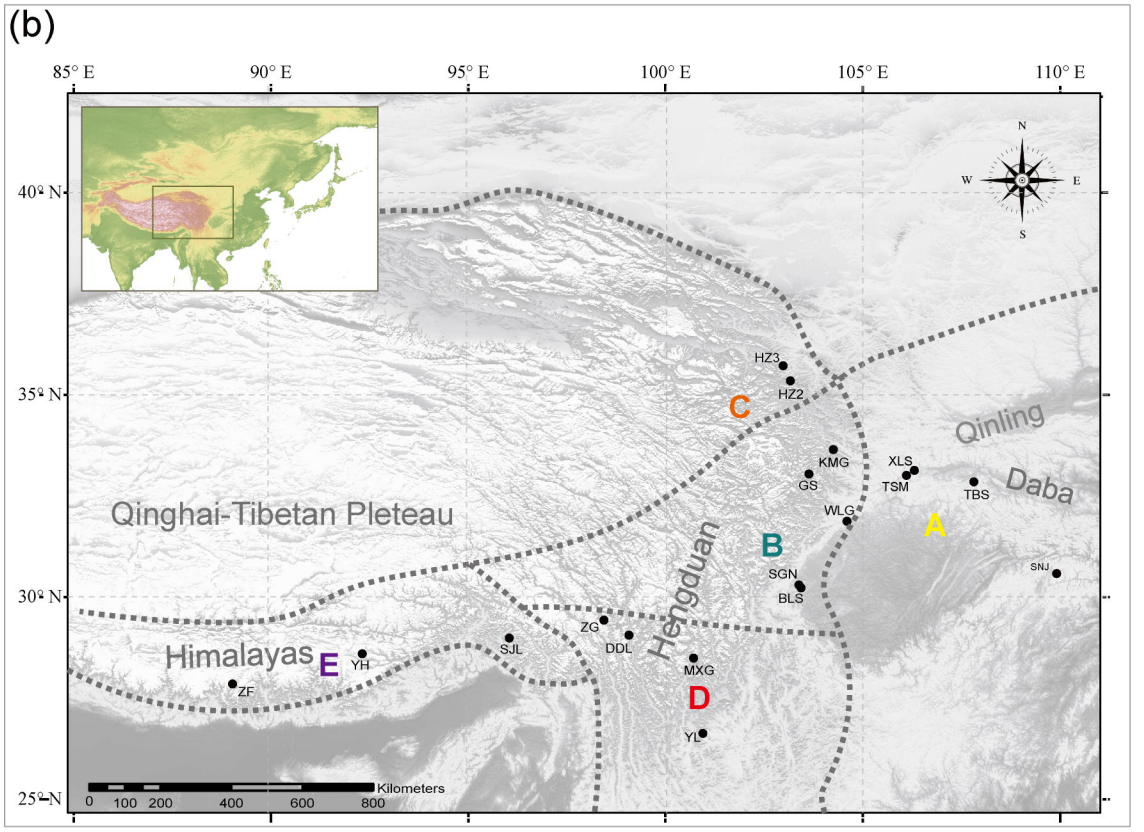

(c)

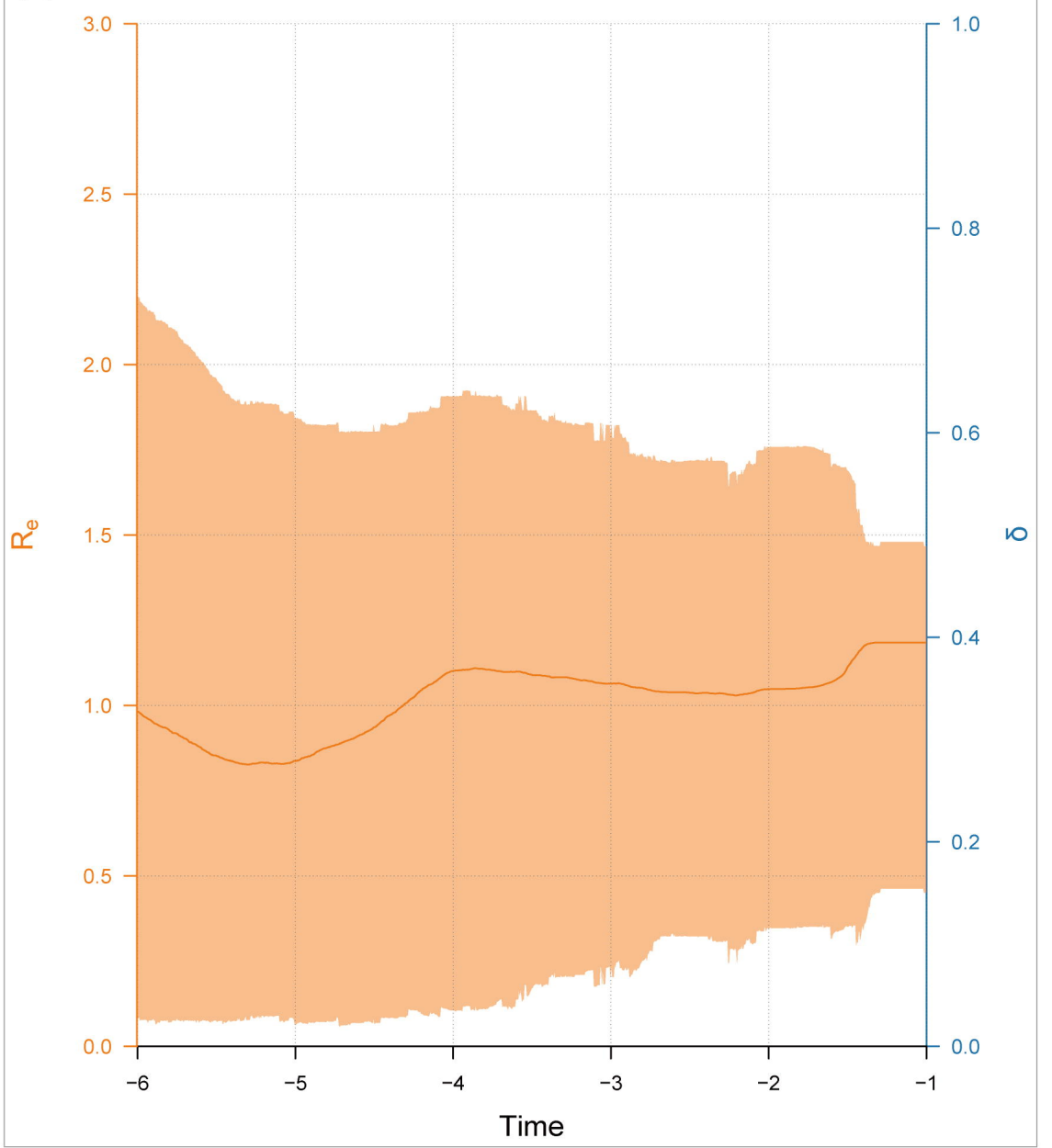

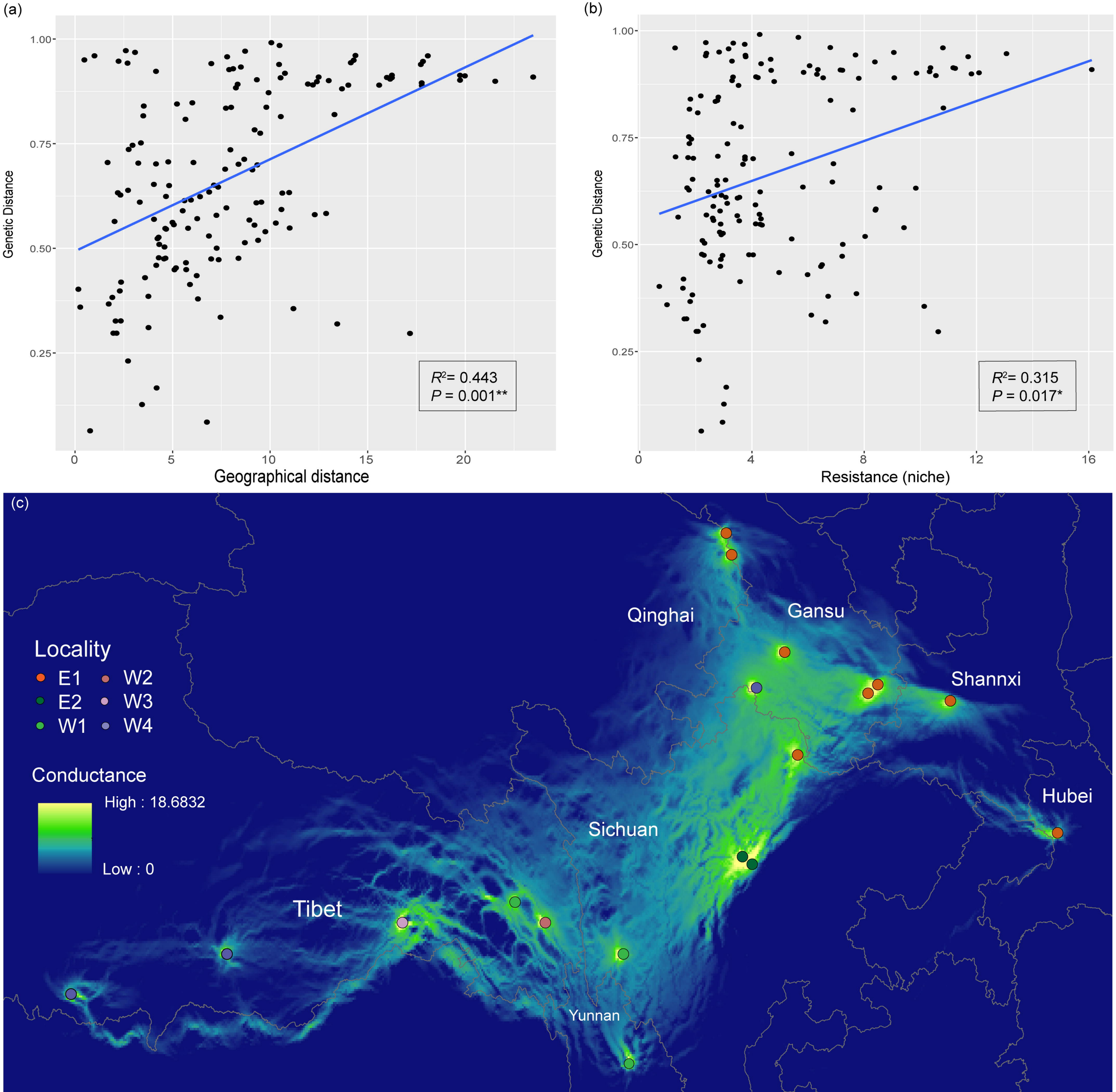
(a)
Genetic Distance
Geographical distance
R^2= 0.443
P = 0.001**
(b)
Genetic Distance
Resistance (niche)
R^2= 0.315
P = 0.017*
(c)
Locality
E1
E2
W1
W2
W3
W4
Conductance
High : 18.6832
Low : 0
Qinghai
Gansu
Shannxi
Hubei
Sichuan
Tibet
Yunnan

(a)

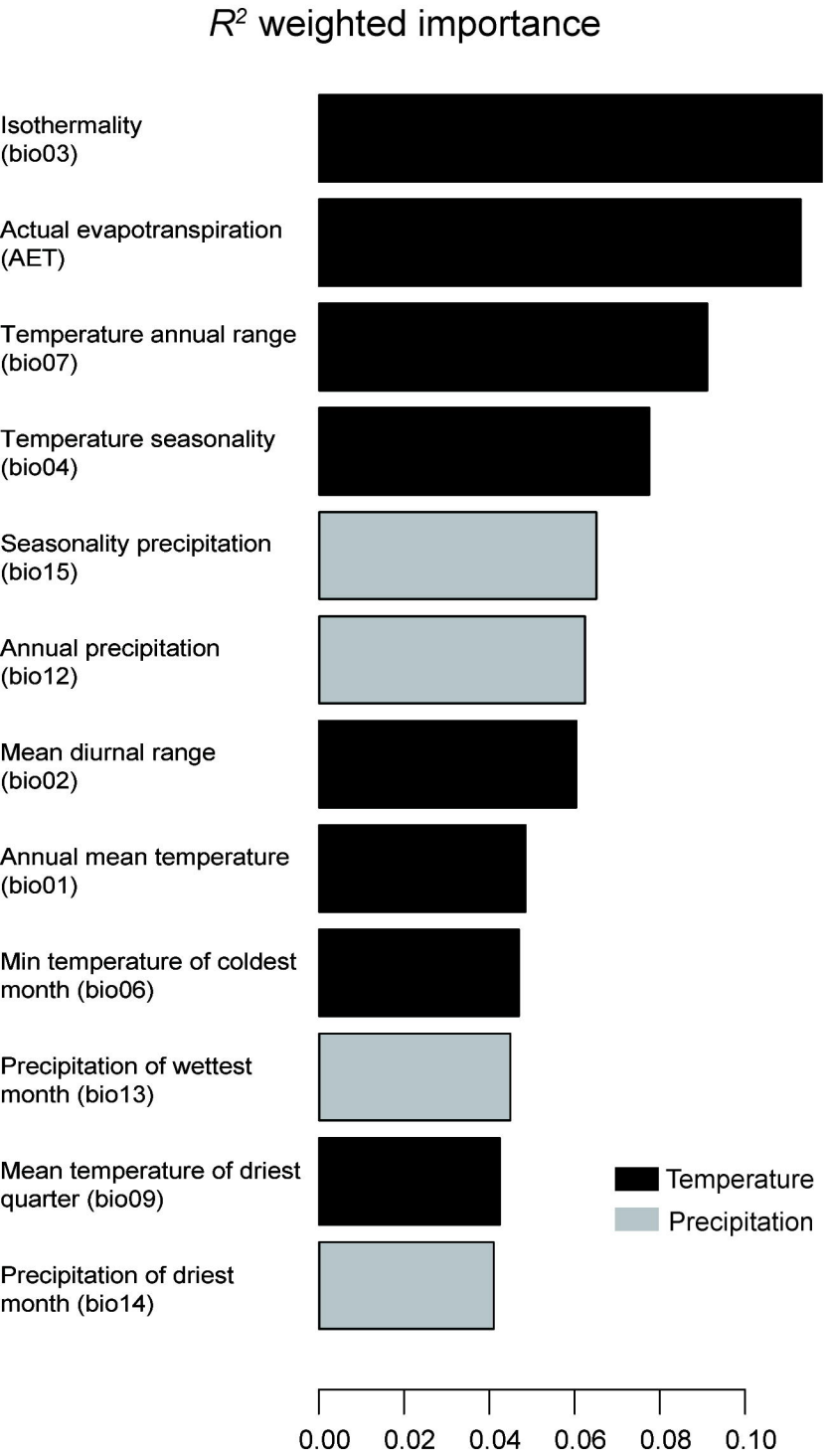
R^2 weighted importance
Isothermality (bio03)
Actual evapotranspiration (AET)
Temperature annual range (bio07)
Temperature seasonality (bio04)
Seasonality precipitation (bio15)
Annual precipitation (bio12)
Mean diurnal range (bio02)
Annual mean temperature (bio01)
Min temperature of coldest month (bio06)
Precipitation of wettest month (bio13)
Mean temperature of driest quarter (bio09)
Precipitation of driest month (bio14)
Temperature
Precipitation
0.00
0.02
0.04
0.06
0.08
0.10

(b)

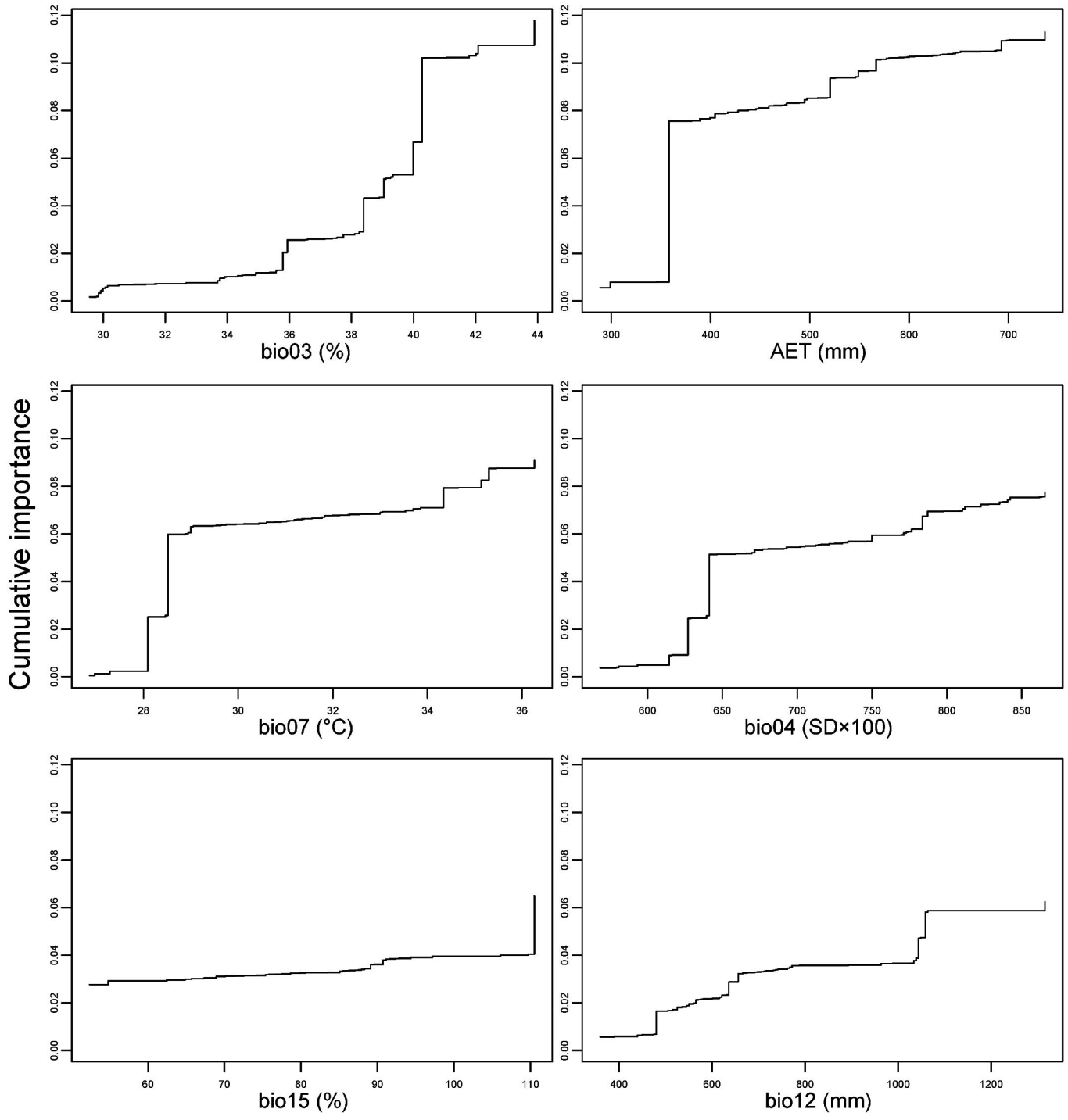
Cumulative importance
bio03 (%)
AET (mm)
bio07 (°C)
bio04 (SD×100)
bio15 (%)
bio12 (mm)

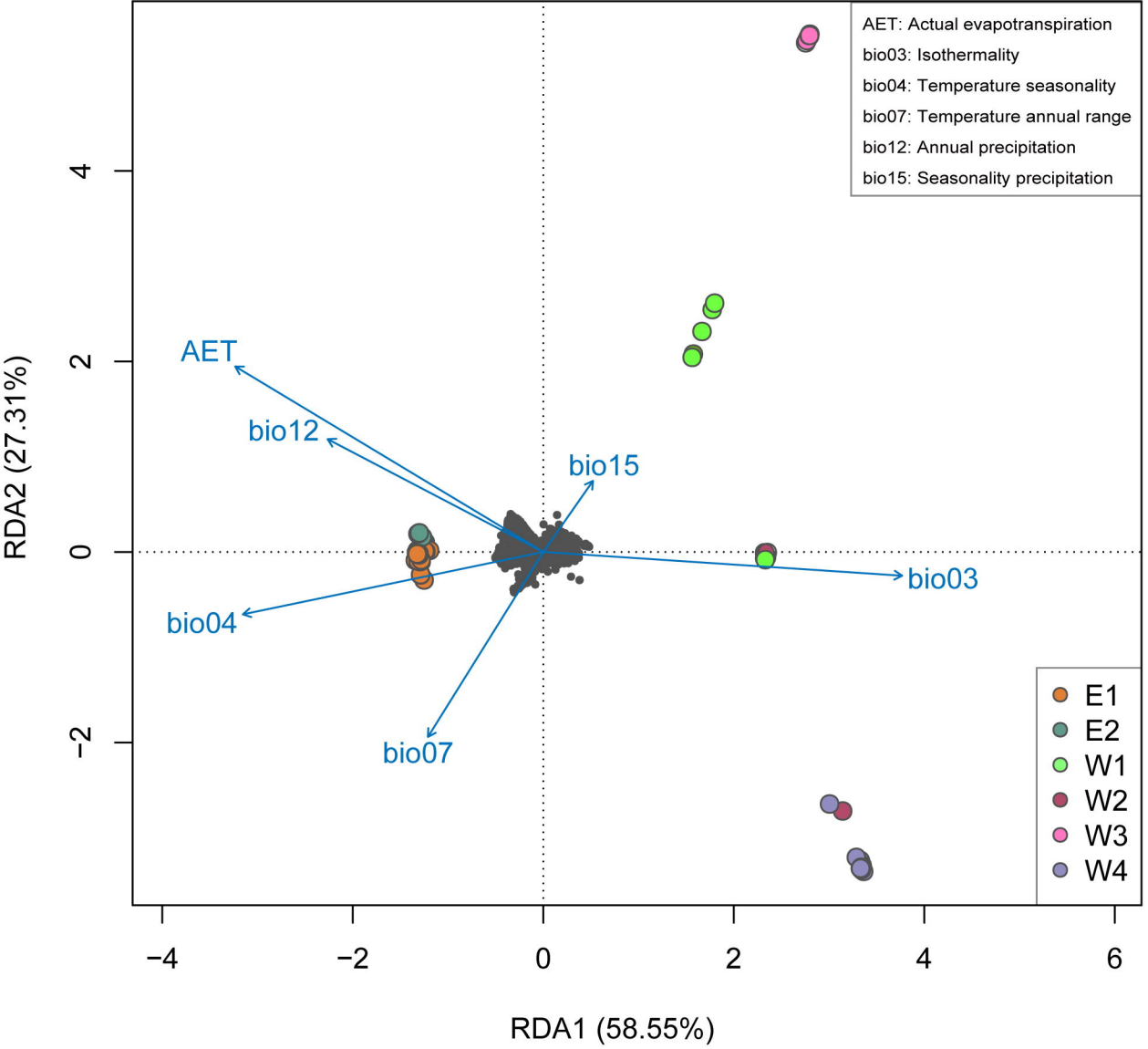
AET: Actual evapotranspiration
bio03: Isothermality
bio04: Temperature seasonality
bio07: Temperature annual range
bio12: Annual precipitation
bio15: Seasonality precipitation
AET
bio12
bio15
bio03
bio04
bio07
E1
E2
W1
W2
W3
W4
RDA2 (27.31%)
RDA1 (58.55%)
−4
−2
0
2
4
6
−2
0
2
4